공학박사학위논문

A study on the optimization of viscoelastic ink and processing conditions for the formation of Taylor cone jet in electrohydrodynamic jet printing

전기수력학적 프린팅 공정에서 테일러 콘 젯 형성을 위한 점탄성 잉크와 공정 조건의 최적화에 대한 연구

2016 년 2 월

서울대학교 대학원

화학생물공학부

유 미 림

Abstract

A study on the optimization of viscoelastic ink and processing conditions for the formation of Taylor cone jet in electrohydrodynamic jet printing

Milim Yu

School of Chemical and Biological Engineering

Seoul National University

Electrohydrodynamic(EHD) jet printing is considered to be a promising tool for making nano-scale patterns as the demand for miniaturization of electronic devices increases. The formation of Taylor cone jet is a key process in EHD jet printing that is used to produce high resolution patterns. It is well known that the formation of Taylor cone jet mainly depends on the processing conditions, geometry conditions, and the liquid properties: elasticity, viscosity,

conductivity, surface tension, and dielectric constant. Especially, even though the viscoelastic inks are complex fluids composed of particles, binder, and solvent, most of previous researches have assumed the ink as a Newtonian fluid. To obtain uniform and high resolution printing products, controlling the physical properties of viscoelastic ink and predicting the processing ranges for Taylor cone jet are very important. In this study, therefore, we design the desired properties of viscoelastic ink and optimize the processing conditions for the formation of Taylor cone jet by investigating the effect of rheological and electrical properties of low viscous elastic fluids, which are suitable materials for EHD jet printing.

Firstly, we organize the seven dimensionless number based on the all parameters involved in the EHD jet printing to systemize the variables affecting the Taylor cone jet. Dimensionless flow rate (α) and dimensionless voltage (β) are used for dimensionless processing condition. Two dimensionless numbers related to physical properties of ink, elastic parameter (ξ) and viscosity parameter (χ), are key parameter that determines whether elasticity and viscosity has an effect on the Taylor cone jet formation, respectively. We controlled the ξ and χ using two model systems designed to control the elasticity and viscosity of the ink independently. The results can be summarized in terms of two parameters: elasticity parameter, ξ,

and viscosity parameter, χ. The increase in elasticity widens the range of voltage for Taylor cone jet zone, while the range of flow rate remains independent of elasticity. Especially, an increase of elasticity increased the initial voltage, the voltage at which the Taylor cone jet first appears. The results demonstrated that elasticity enhanced the inward direction of normal stress on the surface of conical shape. The effect of elasticity is dominant for $\xi > 1$ while it is nearly negligible for $\xi < 1$. When the viscosity is increased, the Taylor cone jet zone widened mainly by the flow rate when $\chi < 1$, while the voltage stabilizes the Taylor cone jet for $\chi > 1$. As a result, the viscoelasticity improves the stability by expanding the processing range for Taylor cone jet.

Secondly, we investigated the effect of the interaction between the electrical and rheological properties of the ink by designing model systems that control both the electrical conductivity and the viscoelasticity of the ink to observe how they affect the Taylor cone jet formation. The ink with high electrical conductivity produced the conical shape with large surface area. It induces a higher initial voltage. The results demonstrated that the large surface area is needed to accumulate sufficient charge for the formation of Taylor cone jet. After forming the Taylor cone jet, the ink with high electrical conductivity increased the final voltage, the voltage at which the jet becomes unstable by

stabilizing the conical shape. When the electrical conductivity increased by the same rate, the voltage ranges for Taylor cone jet decreased as the ink's viscoelasticity increased. The results implied that the viscoelasticity obstructs the charge transport to the surface of conical shape. Consequently, increased viscosity and elasticity also lead to the similar result with increase of electrical conductivity: increase of the initial and final voltages, which can be attributed to the slower charge transport that minimizes the stabilizing effect of the inks' electrical conductivity.

This study suggests guidelines for optimization of the process parameter and design of desired properties of the viscoelastic ink to produce Taylor cone jet. All variables affecting the EHD jet process are systemized by dimensional analysis. The effect of rheological and electrical properties of viscoelastic ink on Taylor cone jet was investigated by designing the model systems. The relationship between the properties of ink and the processing conditions for Taylor cone jet is shown through the processing window maps by using the dimensionless processing conditions, dimensionless flow rate (α), and dimensionless voltage (β). This study will contribute to the optimal design of viscoelastic ink and processing conditions on the formation of Taylor cone jet in EHD jet printing.

Keywords: Electrohydrodynamic jet printing, Taylor cone jet, Viscoelastic ink, Rheological property, Electrical conductivity, Dimensionless parameter, Processing window map, High resolution pattern

Student Number: 2008-22982

Contents

List of Figures

List of Tables

Chapter 1.

Introduction

1.1. General introduction

The core principle of electrohydrodynamic (EHD) jet printing is the formation of the cone jet which is generated by an electric potential between the nozzle and the substrate. The electric stress caused by the electric potential can change the shape of the ink from droplet to conical shape known as "Taylor cone" [Zeleny (1914), Hayati et al. (1986), Taylor (1964)]. The electrified jet, which has much smaller diameter than the nozzle diameter, can be produced and printed by forming Taylor cone jet, while the droplet diameter from the ink jet printing swells 2 to 3 times larger than the nozzle diameter.

Finding the proper processing conditions is of a great importance in obtaining a stable Taylor cone jet. It is very challenging because the formation of Taylor cone jet and the printing quality are affected by many factors as follows: processing factors (flow rate, voltage) [Ganan-Calvo (2009), Yordem et al (2008), Wei et al (2013), Gamero-Castano (2002), Lee et al. (2012)]; geometry factors (nozzle diameter, distance between nozzle and substrate) [Barrero et al (1999), Khan et al. (2012)]; the physical properties of the ink (viscoelasticity [Reneker et al. (2008), Carroll et al (2006), Mestel (1996)], viscosity [Kim et al. (2014), Kang et al (2011)], conductivity [Fernandez de la

Mora (1992), Helgeson et al. (2008), Theron et al. (2004)], surface tension [Lee et al. (2012)], dielectric property [Conroy et al. (2011), Chen et al. (1997)], density). The physical properties of the ink, in specific, influence the stability of Taylor cone jet, which is an outcome of multidisciplinary subjects of electrostatics, electrokinetics and fluid dynamics [Ganan-Calve (1997)].

The studies on the role of fluid properties on the Taylor cone jet have been performed for many years. While previous studies have observed the role of physical properties on the morphology and the instability of the Taylor cone jet, most of them did not consider the interaction of multiple factors on the formation of the Taylor cone jet [Yu et al. (2007), Luo et al. (2012), Angammana et al (2011), Stanger et al (2009)]. In industrial applications, many parameters are involved and affect each other. In this sense, the previous studies on the role of a single property have limitations in predicting the Taylor cone jet formation in industrial processes. As the ink includes functional particles and polymers, it can be classified as a complex fluid [Korkut et al. (2008), Bober et al. (2011)].

The viscoelasticity of the ink can induce many unexpected phenomena in printing process, thus it should be included as a key material property together with all the associated factors that affect EHD jet printing process. Nonetheless, most researches on EHD jet printing have assumed the ink as a simple

Newtonian fluid [Bober et al. (2011), Lee et al. 2013)]. A few researches have been considered viscoelastic inks, but the effect of elasticity and viscosity has never been probed separately. Moreover, a few others investigated the role of rheological properties of the ink, but did not consider the role of fluid electrical property altogether [Yang et al. (2010), Carroll et al (2008), Regev et al. (2010)]. The electrical property of the ink is also an important factor in the formation of Taylor cone jet as it induces the tangential stress on the surface of Taylor cone jet [Mora (2007), Hartman et al. (1999), Barrero et al. (1999)].

Therefore, in this study, we explored the effect of viscoelasticity on the formation of Taylor cone jet using the well-characterized model systems of low viscosity elastic polymer solutions. Two model systems were designed such that elasticity and viscosity varied independently, while all the other material properties were kept constant.

In addition, we examine the influence of the electrical property depending on the rheological properties. To consider the effect of the interaction between the electrical property and the rheological properties, we make a processing window map for the Taylor cone jet when both the electrical and rheological properties are varied. To achieve the goal, we design three rheologically distinct inks: an ink with low elasticity and low viscosity, one with high elasticity and low viscosity, and finally an ink with low elasticity and high

viscosity. By altering the electrical conductivity in these three rheologically different inks, we discuss the effect of the electrical conductivity on the Taylor cone jet formation depending on the rheological properties.

Furthermore, to optimize between processing condition and physical properties of ink, all the variables associated in EHD jet printing process were restructured systematically in terms of seven dimensionless numbers.

Finally, we plotted the processing window maps for all sets of model fluids by utilizing the dimensionless parameters. As the rheological and electrical properties of the ink changed in each system, the optimum processing condition for the Taylor cone jet formation was determined quantitatively in terms of dimensionless numbers.

1.2. Outline of the thesis

In chapter 2, the background of the thesis will be described. It is divided into EHD jet printing and Taylor cone-jet transition. The first part of chapter 2 describes about the process and application of EHD jet printing. The second part of chapter 2 explains the definition, evolution, mechanism, and application of the Taylor cone-jet transition.

In chapter 3, theoretical background will be presented in term of design of dimensionless groups related to EHD jet printing. Seven dimensionless parameters are organized as a systematic approach to find the process windows and to apply to the printing system.

In chapter 4, the information of materials and characterization will be described. The model systems for control of rheological and electrical properties of ink will be introduced in this part.

In chapter 5, main results and discussion of the research are explained by well-defined model system and processing window maps for each model systems.

In chapter 6, the results on the work about the design and optimization of EHD jet printing process are summarized.

Chapter 2.

Background

2.1. Electrohydrodynamic jet printing

Electrohydrodynamic jet printing is high resolution printing approach, in which the liquid is subjected to electrostatic field to form a Taylor cone jet. Industry insiders have considered it as an alternative process to inkjet printing because it can overcome the inherent limitation of the conventional inkjet printing associated with the size of a nozzle, which determines high resolution patterning [Park et al. (2010), Khan et al. (2012), Lee et al. (2012)].

EHD jet printing is a complex process which reflects the multidisciplinary approach of fluid dynamics, electrostatics and electrokinetics. The liquid is supplied to the capillary tube using a syringe pump. A high voltage is applied between a conducting nozzle and a substrate. The jetting mode is determined by three forces; hydrodynamic force which supplies more fluid to emerging droplet, capillary force which tends to keep the droplets at the end of the nozzle, and electrostatic force which is caused by electric field [Joffre and Cloupeau (1986), Li (2006)].

It is applicable in various fields such as printed electronics [Park et al. (2007), Wang et al. (2009)], solar cell [Muhammad et al. (2011), Park et al. (2011)], biological sensors [Park et al. (2008)], tissue engineering [Hashimdeen et al. (2014), Kim et al. (2014)] and many more.

2.2. Taylor cone jet

2.2.1. Definition of cone-jet transition

The liquid is formed to droplet shape on the tip of the capillary tube because of surface tension as seen in Fig 2.1(a). The droplet is transformed into a conical shape by applying the electric field when the electric stress surpasses the surface tension. The conical shape was first reported by Zeleny in 1914 and named as Taylor cone in 1964 [Zeleny (1914), Taylor (1964)]. In theory, a perfect Taylor cone has a whole angle of 98.6^{o} before jet formation. When a certain threshold voltage has been reached, jet is emitted from end of the cone shape as in Fig. 2.1(b). This is called a cone-jet transition.

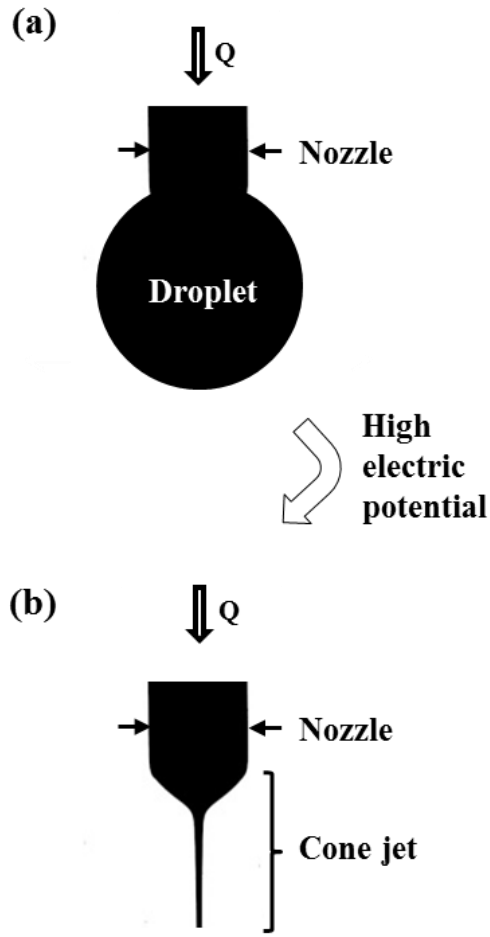

Figure 2.1. Schematic illustration of the cone-jet transition where electric potential induces the change of liquid shape from droplet to cone jet: (a) droplet shape with no electric potential, (b) conical shape with high electric potential.

2.2.2. Evolution

According to the relationship between surface tension and electric stress, there are various jetting mode, such as dripping mode, pulsating mode, cone-jet mode, tilted mode, twin mode and multi-jet mode. Classical jetting evolution of Newtonian fluid in EHD jet printing are shown in Fig. 2.2.

At zero voltage, the liquid is dripped from the nozzle because of surface tension. If an electric potential is gradually applied to a capillary, the size of the drop decreases while the dripping rate increases. The imbalance of the surface tension and electric stress induces the pulsating mode which is repeating the hemispherical shape and Taylor cone shape. At a critical potential, the drop develops into a Taylor cone shape with a fine stable jet. When larger voltage is applied after Taylor cone jet, unstable cone jet shapes are occurred such as twin and multi-jet [Cloupeau et al. (1994), Jaworek and Krupa (1999), Chen et al. (2005), Yurteri et al (2010), Lee et al. (2013)].

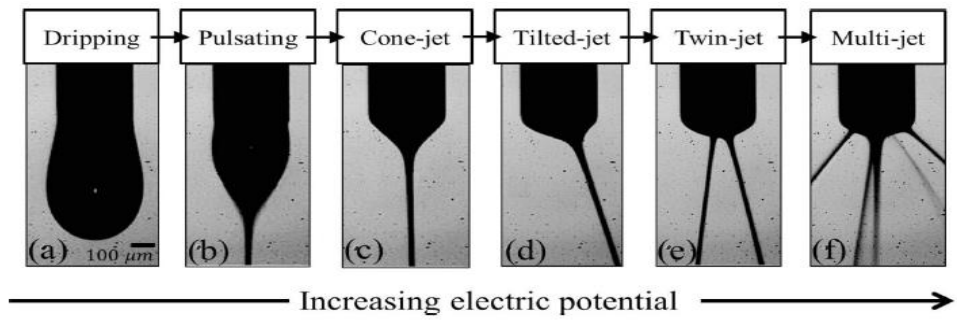

Figure 2.2. Electrohydrodynamic jetting modes with respect to electric potential [Lee et al. (2013)]

2.2.3. Mechanism

A voltage difference is applied between the capillary nozzle and the substrate to create an electric field around the fluid. Electric charge and electric stress are induced by electric field in the liquid surface. Electric charge accumulates at liquid surface and leads to creation in the normal and tangential direction to the outward electric tangential stress. Electric tangential stress competes with electric normal stress. When normal electric stress is balanced with the corresponding normal direction stress such as surface tension to the inside of liquid surface, Taylor cone jet can be formed by electric tangential stress [Zeleny (1914), Taylor (1964), Mora (2007), Higuera (2008)]. Normal electric stress destabilizes the cone jet while tangential electric stress stabilizes the interface of cone jet. The force exerted on the surface of cone jet is shown in Fig. 2.3.

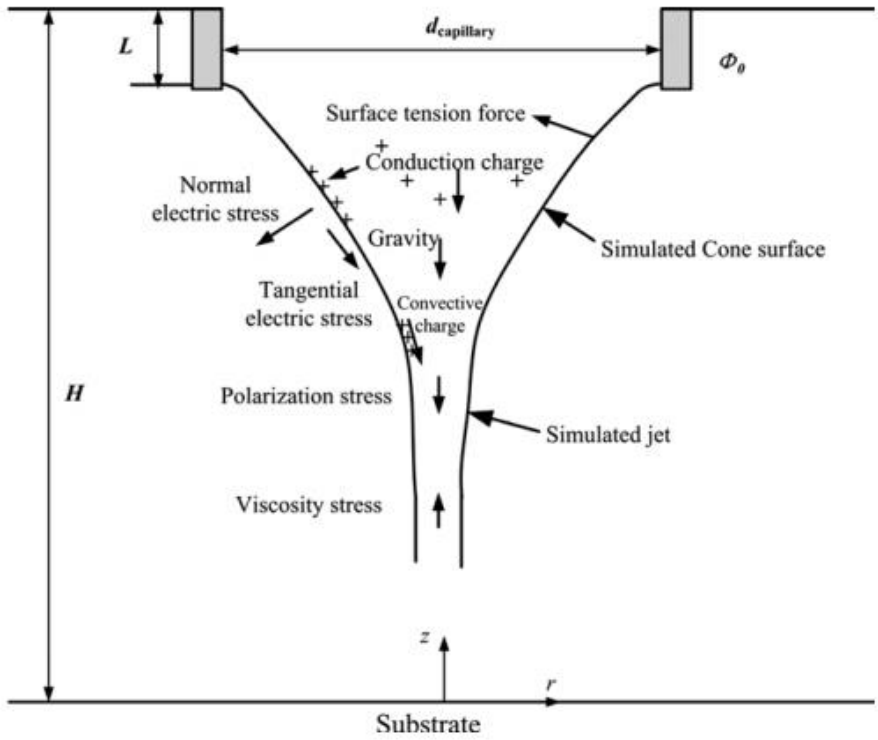

Figure 2.3. The schematic of electrode configuration and force exerted on the cone-jet [Wei et al. (2013)]

2.2.4. Application

Taylor cone jet has been applied in many applications such as electrospinning, electrostatic spraying and electrohydrodynamic jet printing. Electrospinning is a simple method to produce polymeric nanofibers as seen in Fig. 2.4. These fibers have the merit of high surface to volume ratio, better surface functionality and high degree of porosity. These characteristics make them useful in filtration devices, drug delivery, fiber with specific surface chemistry and scaffolds useful in tissue engineering [Qin et al. (2006), Hu et al. (2014), Lannutti et al. (2007)]. Electrostatic spraying produces charged droplets as seen in Fig. 2.5. The charge and size of droplets can be controlled by using the various jetting modes as function of processing conditions. The most ideal electrospray mode is the cone jet mode which produces monodisperse size distribution while the micro-dripping and multi-jet mode induce a broad droplet size distribution. Charged droplet generated by cone jet mode allows production of micron-sized droplets that can be applied in the technology of nano-particles of for the deposition of thin solid films [Jaworek et al. (2009), Jose et al. (2015)].

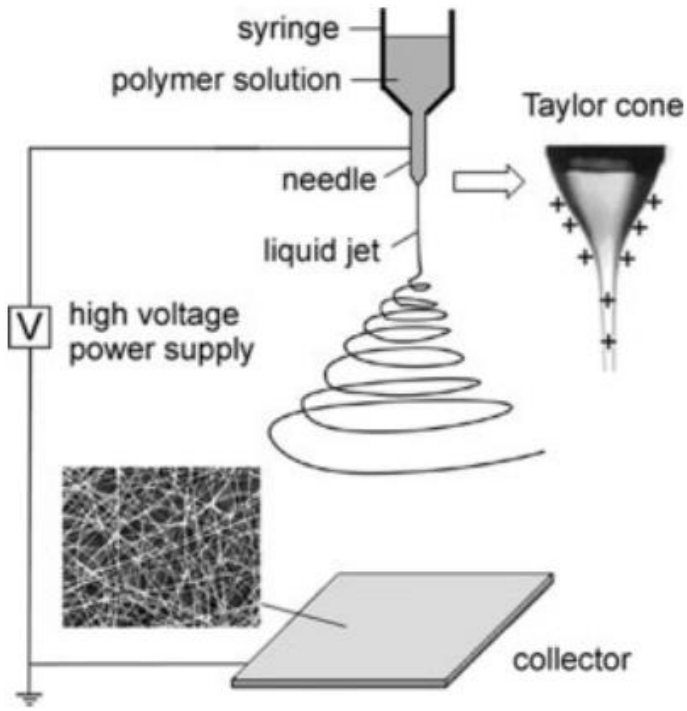

Figure 2.4. Schematic illustration of the basic setup for electrospinning. The insets show a drawing of the electrified Taylor cone and a typical SEM image of the nonwoven mat of poly(vinyl pyrrolidone) (PVP) nanofiber deposited on the collector [Li et al. (2004)].

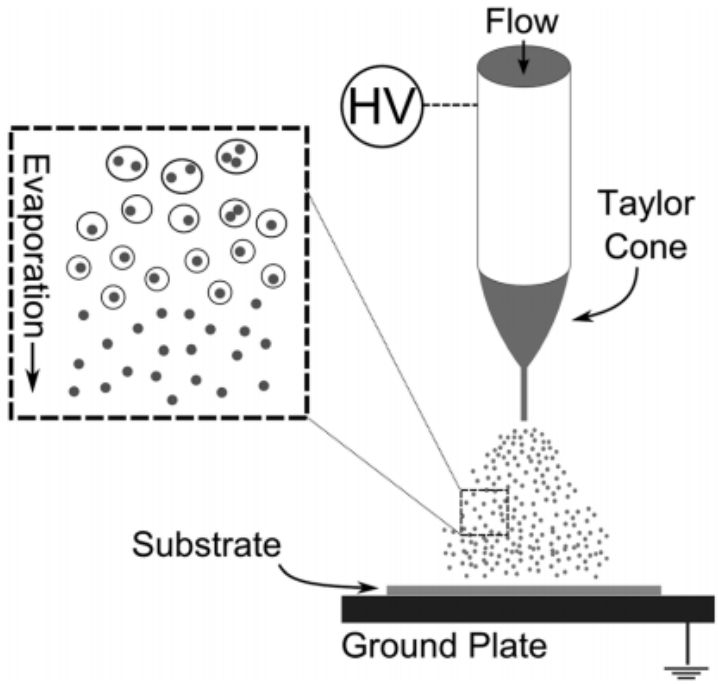

Figure 2.5. Electrospray of colloidal dispersion. The high electric potential deforms fluid at the edge of the capillary tube in to a Taylor cone. A jet emits from the apex of the cone and breaks up in to charged droplets. The droplets rapidly evaporate, leaving dry material that is deposited on to the substrate [Brown et al. (2015)].

Chapter 3.

Theory

3.1. Design of dimensionless groups in EHD jet printing

3.1.1. Influence factors

EHD jet printing process and Taylor cone jet are affected by many factors such as processing condition, geometric condition and properties of ink. The factors are listed in the Table 3.1.

Many studies have been devoted to the determination of the physical laws relating the cone jet formation. However, most results were focused on the simple relationship between jet diameter and printing parameters which are the processing conditions and liquid properties. Some researchers have been attempted to consider the all parameters involved in the EHD jet printing, but the studies were limited to numerical analysis and Newtonian fluid [Lee et al. (2013)]

In the following section, all the variables associated in Taylor cone jet including viscoelasticity were restructured systematically in terms of seven dimensionless numbers.

Table 3.1. Major factors influencing Taylor cone jet

Processing conditions	**Geometric conditions**	**Physical properties of ink**
Q - Flow rate V - Voltage	d - Diameter of nozzle L - Distance between nozzle and substrate	λ - Relaxation time η - Viscosity κ - Conductivity γ - Surface tension ε' - Permittivity

3.1.2. Dimensional analysis

Dimensionless numbers were organized to systemize all the variables that affect the EHD jet printing. Using the Buckingham π theorem, the number of dimensionless groups could be determined as the number of variables minus the number of fundamental dimensions. The variables are:

$$Q,\ V,\ \lambda,\ \eta,\ \kappa,\ \gamma,\ \rho,\ \varepsilon',\ \varepsilon_o,\ d,\ L \tag{3.1}$$

where Q is the flow rate, V is the voltage, λ is the Zimm relaxation time, η is the viscosity, κ is the conductivity, γ is the surface tension, ρ is the density, ε' is the permittivity of fluid, ε_o is the permittivity of the surrounding air, d is the diameter of the nozzle, and L is the separation distance of the nozzle and the counter-electrode. As eleven variables contain four fundamental dimensions, $[M]$, [L], $[T]$ and $[V]$, seven dimensionless numbers could be derived and the results are summarized in Table 3.2.

Table 3.2. Dimensionless numbers that govern the EHD jet printing process

Processing conditions		**Geo-metry**	**Physical properties of ink**			
α	β	L/d	ξ	χ	σ	ε'
$\frac{\rho\kappa Q_s}{\varepsilon'\varepsilon_o\gamma}$	$\sqrt{\frac{\varepsilon_o}{\gamma d}}V_a$	L/d	$\sqrt{\frac{\gamma}{\rho d^3}}\lambda$	$\left(\frac{\kappa}{\gamma^2\rho\varepsilon'\varepsilon_0}\right)^{1/3}\eta$	$\sqrt{\frac{\rho d^3}{\gamma}}\frac{\kappa}{\varepsilon'\varepsilon_o}$	ε'
$=\frac{Q_s}{Q_c}$	$=\frac{V_a}{V_c}$	L/d	$=\frac{t_\lambda}{t_\gamma}$	$\left(\frac{\kappa}{\gamma^2\rho\varepsilon'\varepsilon_0}\right)^{1/3}\eta$	$=\frac{t_\gamma}{t_c}$	ε'

Dimensionless flow rate (α) and dimensionless voltage (β) are the main process parameters. α is defined as the ratio of supplied flow rate (Q_s) to critical flow rate (Q_c). Q_s is the flow rate supplied experimentally by the syringe pump, and Q_c is the minimum flow rate required for steady cone jet formation, which is defined as follows [Fernandez de la Mora et al. (1994)] :

$$Q_c = \frac{\gamma \varepsilon' \varepsilon_o}{\rho K} \tag{3.2}$$

β is the ratio of applied voltage (V_a) to critical voltage (V_c). V_a is the experimentally applied voltage, and V_c is the critical voltage that supports the meniscus on the nozzle of diameter d as follows [Taylor (1964)] :

$$V_c = \sqrt{\frac{\gamma d}{\varepsilon_o}} \tag{3.3}$$

The required condition for the formation of stable jet is satisfied when α and β are larger than 1.

L/d is the geometry parameter. It is defined as the ratio of the distance between the nozzle and the substrate (L), and the nozzle diameter (d).

ξ, χ, σ and ε' depend only on the physical properties of the liquid and not on the processing conditions. ξ is a new dimensionless number which we firstly propose to characterize the elasticity of the ink. It is defined as the ratio of the Zimm relaxation time to capillary time (t_λ / t_γ).

$$\xi = \frac{\lambda}{\sqrt{\rho d^3/\gamma}} = \frac{t_\lambda}{t_\gamma} \tag{3.4}$$

The Zimm relaxation time represents how long a single polymer chain takes to relax, reflecting the elasticity of the ink. Capillary time represents the jetting time required to eject enough charge, and is estimated as $t_\gamma = (\rho d^3/\gamma)^{0.5}$ [Bober et al. (2011)].

χ is a dimensionless number that represents the effect of viscosity, which is composed of two characteristic velocities. $\eta/\rho d$ is the propagation velocity of a perturbation by viscous diffusion, and Q_c/d^2 is the characteristic velocity of the fluid [Lee et al. (2013)].

$$\chi = \frac{\eta}{(\rho\gamma^2 \frac{\varepsilon' \varepsilon_o}{\kappa})^{1/3}} = \frac{\eta/\rho d}{Q_c/d^2} \tag{3.5}$$

σ is the ratio of capillary time (t_γ) to the electrical charge relaxation time (t_c), where t_c is the characteristic time of the charge transport determined by the electrical properties of the fluid. ε' is the permittivity of the fluid which relates the degree of dipole alignment.

Chapter 4.

Experimental section

4.1. Materials and characterization

The low viscosity elastic fluids tested in this study were dilute solutions of polyethylene oxide (PEO) (supplied by Aldrich Chemical) with molecular weight ranging from 3.0×10^5 to 5.0×10^6 in $55\ wt\%$ water/ $45\ wt\%$ glycerol mixture. Polymer solutions were prepared at various concentrations of PEO and NaCl to obtain a wide range of solution properties. Triton X-100 (supplied by Aldrich Chemical) was added to control surface tension of solution. Polymer solutions were stirred for 72 hours using a magnetic stirrer. The shear viscosities of PEO solutions were measured using a strain-controlled rotational rheometer (ARES, TA instruments, USA) with a conical fixture of $50\ mm$ diameter and 0.04 radian cone angle. The viscosity of PEO solution with molecular weight $5.0\times10^6\ g/mol$ showed slight shear thinning. Other polymer solutions showed constant viscosity in the shear rate range from 1 to $100\ s^{-1}$. Dielectric analyzer (SI 1260, Solartron, U.K.) was used to measure conductivity and permittivity. Surface tension was measured using a surface tensionmat (Fisher Scientific, U.K.).

4.2. Model systems

Three model systems were designed to analyze a) the effect of elasticity (model system I), b) the effect of viscosity (model system Ⅱ) and c) the effect of conductivity (model system Ⅲ) independently. The concentration of ink was adjusted within the semi-dilute regime where the stable jet can be generated without spinning or bead jet [Gupta et al. (2005), Shenoy et al. (2005), Daga et al. (2006), Son et al. (2004)].

4.2.1. Effect of rheological properties

4.2.1.1. Effect of elasticity (model system Ⅰ)

In the first model system, the elasticity of the ink was controlled by changing polymer relaxation time which practically reflects the elasticity. The relaxation time in the semi-dilute region was estimated by the Zimm relaxation time, which can be calculated from the molecular weight and solvent viscosity [Tirtaatmadja et al. (2006)]. Because of constant solvent viscosity in this system, the Zimm relaxation time depends only on the molecular weight of the polymer. Six PEO solutions with different molecular weight were prepared and their viscosity were adjusted to be constant by fixing the reduced concentration, $c/c^* \sim 2.2 \pm 0.2$, where c^* is the critical overlap concentration (explained in Table 4.1). The material properties of the model inks are listed in Table 4.1. Here, for example, M10 means the PEO solution of molecular weight 1.0×10^6 g/mol. The text in parenthesis refers to unit.

Table 4.1. Model system I. Characteristic properties of PEO solutions with various molecular weight: molecular weight (M_w), dimensionless concentration (c/c^*), Zimm relaxation time (λ), zero shear viscosity (η_0), electrical conductivity (κ) and surface tension (γ).

Code name	M_w (g/mol)	c/c^*	$\lambda = t_\lambda$ (s)	η_0 (cp)	κ $(\mu S/cm)$	γ (mN/m)
M03	3.0×10^5	2.13	5.1×10^{-5}			
M06	6.0×10^5	2.33	1.6×10^{-4}			
M10	1.0×10^6	2.16	3.7×10^{-4}	22.0	24.0	56.0
M20	2.0×10^6	2.34	1.2×10^{-3}	$\pm$2.3	$\pm$1.8	$\pm$2.5
M40	4.0×10^6	2.42	4.2×10^{-3}			
M50	5.0×10^6	2.41	5.3×10^{-3}			

* Critical overlap concentration (c^*) was calculated by classification of Flory for flexible polymer solutions, which is defined as $c^* = 1/[\eta]$ [Tirtaatmadja et al. (2006), Graessley et al. (1980)]. It is widely accepted for dilute and semi-dilute polymer solutions. $[\eta]$ is the intrinsic viscosity of polymer solution which depends on the molar mass of the chain according to the Mark-Houwink-Sakurada equation, where $[\eta] = 0.072 M_W^{0.65}$ for PEO solution in water/glycerol mixture [Tirtaatmadja et al. (2006)].

4.2.1.2. Effect of viscosity (model system Ⅱ)

In the second model system, the viscosity of the ink was controlled by changing polymer concentration. Six PEO solutions of different concentration were prepared and their elasticity were adjusted to be constant by fixing the molecular weight of PEO ($M_w = 1.0 \times 10^6\ g/mol$). The material properties of the model inks are listed in Table 4.2. Here, for example, C18 indicates the PEO solution of $0.18\ wt\%$.

In model system Ⅰ and Ⅱ, other physical properties of the inks were controlled to be almost the same. The conductivity was fixed by controlling the amount of salt addition. Dielectric constant and surface tension were constant because they are determined by the solvent. The addition of a small amount PEO had no effect on the surface tension and the dialectic constant. Relative permittivity (ε') were maintained at 79.1 ± 2.7 for all the inks.

Table 4.2. Model system Ⅱ. Characteristic properties of PEO ($M_w = 1.0 \times 10^6\ g/mol$) solutions with various polymer concentration

Code name	M_w (g/mol)	c/c^*	$\lambda = t_\lambda$ (s)	η_0 (cp)	κ $(\mu S/cm)$	γ (mN/m)
C18		1.02		9.5		
C24		1.37		12.8		
C30	1.0	1.71	3.7×10^{-4}	17.8	13.0	56.0
C38	$\times10^6$	2.21		24.0	$\pm$2.3	$\pm$2.5
C42		2.40		29.3		
C52		2.97		36.9		

4.2.2. Effect of electrical property

4.2.2.1. Effect of conductivity (model system Ⅲ)

In third model system, the conductivity of the ink was controlled by adding salt. Firstly we used PEO with low molecular weight ($1.0\times10^6\ g/mol$) to formulate the inks with low elasticity. By adding salt to this ink, we designed inks with five different electrical conductivity (with the same elasticity and viscosity), named model system Ⅲ-1 as shown in Table 4.3.

Secondly, PEO of high molecular weight ($5.0\times10^6\ g/mol$) was used to fabricate the samples with high elasticity, named model system Ⅲ-2 (Table 4.4). Because the model system Ⅲ-1 and Ⅲ-2 have significantly different Zimm relaxation time, the analysis of their behavior can show how the conductivity affects the Taylor cone jet formation depending on the ink's elasticity.

Lastly, Model system Ⅲ-3 (Table 4.5) was prepared with higher concentration of PEO than model system Ⅲ-1, yielding the samples with higher viscosity than model system Ⅲ-1. Because both systems utilized PEO of the same molecular weight ($1.0\times10^6\ g/mol$), their elasticities are equal. Therefore, comparative analysis of model system Ⅲ-1 and Ⅲ-3 would reveal

the influence of the conductivity on the Taylor cone jet formation depending solely on the ink's viscosity.

Table 4.3. Model system Ⅲ-1. Characteristic properties of PEO ($M_w = 1.0 \times 10^6\ g/mol,\ 0.32\ wt\%$) solutions with various conductivity

Code name	M_W (g/mol)	c/c^*	$\lambda = t_\lambda$ (s)	η_0 (cp)	κ $(\mu S/cm)$	γ (mN/m)
M10K20					20.4	
M10K40					39.9	
	1.0		3.7	22.0		56.0
M10K60		1.82			59.8	
	$\times 10^6$		$\times 10^{-4}$	$\pm$ 1.7		$\pm$2.5
M10K80					82.1	
M10K100					100.1	

Table 4.4. Model system Ⅲ-2. Characteristic properties of PEO ($M_w = 5.0\times10^6\ g/mol,\ 0.12\ wt\%$) solutions with various conductivity

Code name	M_W (g/mol)	c/c^*	$\lambda = t_\lambda$ (s)	η_0 (cp)	κ ($\mu S/cm$)	γ (mN/m)
M50K20					22.1	
M50K40					24.2	
	5.0		5.3	24.0		56.0
M50K60		1.93			60.9	
	$\times10^6$		$\times10^{-3}$	$\pm$ 2.3		$\pm$2.5
M50K80					80.5	
M50K100					101.4	

Table 4.5. Model system Ⅲ-3. Characteristic properties of PEO ($M_w = 1.0 \times 10^6\ g/mol,\ 0.52\ wt\%$) solutions with various conductivity

Code name	M_W (g/mol)	c/c^*	$\lambda = t_\lambda$ (s)	η_0 (cp)	κ $(\mu S/cm)$	γ (mN/m)
C52K20					21.3	
C52K40					42.3	
	1.0		3.7	39.0		56.0
C52K60		2.95			59.6	
	$\times 10^6$		$\times 10^{-4}$	$\pm$ 2.1		$\pm$2.5
C52K80					79.9	
C52K100					100.4	

Here, for example, M10K20 signifies the PEO solution of the molecular weight $1.0\times10^{6}\ g/mol$ and the conductivity about $20\ \mu S/cm$. C52K20 refers to the PEO solution with high viscosity ($0.52\ wt\%, 1.0\times10^{6}\ g/mol$) and the conductivity about $20\ \mu S/cm$. The conductivity was rounded off for more convenient classification. The text in parenthesis refers to the units.

In model system Ⅲ, dielectric constant and surface tension were constant because they are determined by the solvent. The addition of a small amount PEO had no effect on the surface tension and the dialectic constant. Relative permittivity (ε') were maintained at 79.1 ± 2.7 for all the inks.

4.3. Apparatus

The schematic diagram of the experimental setup is shown in Fig. 4.1. The liquid is supplied to the stainless steel capillary nozzle (inner diameter $180\ \mu m$ and outer diameter $300\ \mu m$) at a constant volumetric flow rate using a digitally controlled syringe pump (Longer Pump , Model LSP02-1B). A high voltage is applied between a conducting nozzle and a copper plate. The working distance between the nozzle and the substrate is $25\ mm$. The jetting mode is observed and simultaneously photographed using a high-speed camera (Photron® fastcam-ultima 512) with 512 512 resolution and micro-zoom lens (6.5X). Light source (MORITEX, 250W Metal Halide lamp) is set up on the opposite side of the camera.

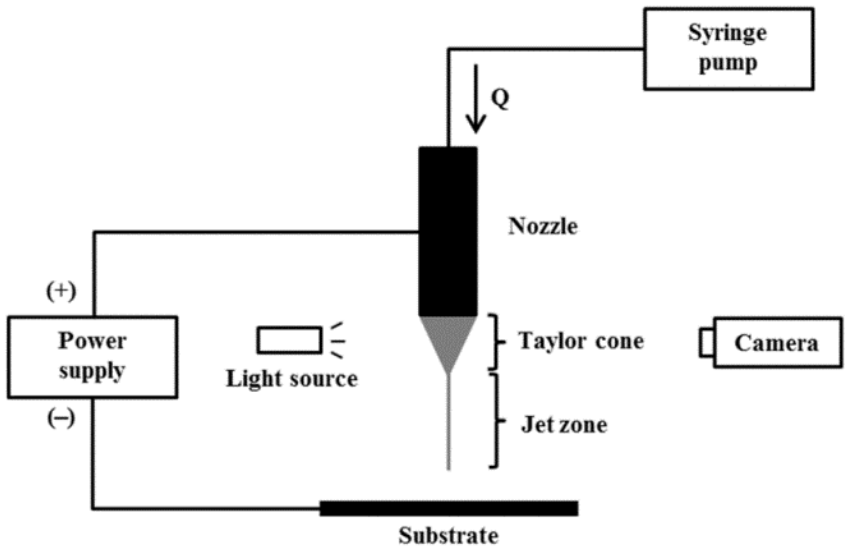

Figure 4.1. Schematics for the EHD jet printing experimental setup

Chapter 5.

Results and discussion

5.1. Characterization of stable cone jet mode

5.1.1. Evolution of jetting mode

The jetting modes of viscoelastic ink were captured and compared with those of the Newtonian ink. We observed the cone-jet evolution of a Newtonian fluid, the mixture of 45 *wt*% glycerol and 55 *wt*% water, and the results are displayed in Fig. 5.1a. The mixture, owing to its high surface tension [Fernandez de la Mora, (2007)], could not proceed to a stable Taylor cone jet after micro-dripping and intermittent cone jet stages even under sufficient flow rate and voltage.

However, after adding 0.38 *wt*% of PEO to the mixture of water and glycerol, many other jetting modes, including the Taylor cone jet, were introduced as seen in Fig. 5.1b. As the voltage increased, the micro-dripping and intermittent jet evolved to Taylor cone jet, and then to tilted jet. Because the stable cone jet was formed by adding a small amount of polymer to the Newtonian fluid, we could expect the viscoelasticity to have positive effect on the formation of Taylor cone jet.

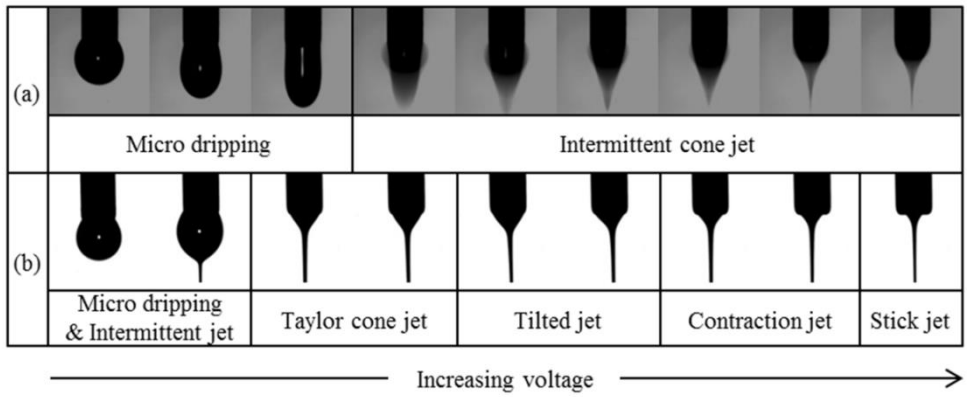

Figure 5.1. Evolution of cone jets: (a) W/G mixture (Newtonian fluid), (b) PEO ($M_w = 1.0 \times 10^6 \ \ g/mol$, $0.38 \ wt\%$) in W/G mixture (viscoelastic fluid).

Two new jetting modes which have not been observed in Newtonian fluid appeared after the tilted jet as illustrated in Fig. 5.1b, named as contraction jet and stick jet. The meniscus of cone shrinks gradually to the center of the jet during the contraction jet mode, and finally stops shrinking, producing the stick jet mode. These results were quite different from the cone jet evolution of the Newtonian fluid at high voltage region. Previous studies, using the Newtonian fluid, reported that high voltage leads to twin or multi-jets [Lee et al. (2012)]. The viscoelasticity in this system prevented the jet to split into two or multi-jets: instead, it caused the meniscus of the cone to shrink.

Evolution of jetting mode was influenced by flow rate as well as voltage. When the flow rate is not in the proper range, Taylor cone jet never formed and unstable jets, such as thin jet and thick jet, were generated. Typical cone jet evolution under insufficient or excessive flow rate was shown in Fig. 5.2a and 5.2b, respectively. In both cases, the cone jet is too thin or too thick, although the appearance of jet evolution was similar to typical evolution of viscoelastic fluid as shown in Fig. 5.1b. When the flow rate was insufficient as in Fig. 5.2a, the upper part of the cone did not completely fill the end of the nozzle, resulting in the formation of thin jet which was not capable of forming a uniform pattern.

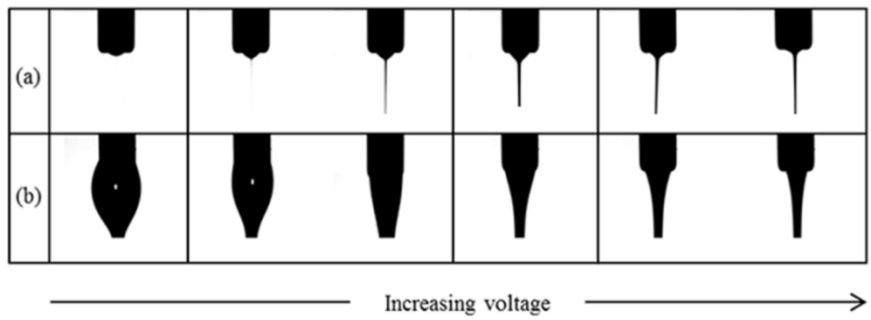

Figure 5.2. Evolution of cone jet of PEO ($M_w = 1.0 \times 10^6 \ \ g/mol$, $0.38 \ wt\%$) in W/G mixture: (a) thin jet from the insufficient flow rate, (b) thick jet from the excessive flow rate.

When the flow rate was excessive as in Fig. 5.2b, the jet diameter becomes too thick to form a high-resolution pattern. A thick jet was defined as the jet diameter was thicker than one third of the nozzle diameter.

5.1.2. Definition of stable Taylor cone jet

In theory, a perfect Taylor cone has a semi-vertical angle of 49.3^{o} before jet formation [Taylor (1964)]. This is called "Taylor angle" and calculated from the balance of capillary and electric pressures under no fluid motion (zero hydrostatic pressure) by Sir Geoffrey Ingram Taylor. Taylor angle derives from the assumption that cone has equipotential surface and cone exists in steady state equilibrium. However, the practical system exist flow and electric fields, so that it has a discrepancy compared to the theoretical one.

In this study, the cone jet is "stable Taylor cone jet" if the following conditions are satisfied.

(1) Meniscus of Taylor cone is not curved line but sharp and straight line.

(2) The jet generated by Taylor cone has straight direction to substrate and there is no instability or spinning at the end of the jet.

(3) The diameter of the jet is thinner than 100 μm.

5.2. Effect of process parameter

5.2.1. Processing condition

Previous studies have revealed that not only the supplied processing conditions but also the physical properties of the inks affect the minimum flow rate and the minimum voltage for the formation of Taylor cone jet in jet printing system.

5.2.1.1. Flow rate

The minimum flow rate (Eq. 3.2) for the formation of Taylor cone jet signifies the specific flow rate caused by the flow of the charge on the Taylor cone jet surface towards the apex due to the applied voltage. Q_c is reported to work well for fluids of relatively high conductivity ($\kappa \geq 1\ \mu S/cm$). This equation is affected by the electrical properties, surface tension and the density of the fluid.

5.2.1.2. Voltage

The critical voltage (Eq. 3.3) is the required minimum voltage to maintain the meniscus when the electric stress deforms the droplet into conical shape. This equation involves the geometry condition (nozzle diameter, d), permittivity and the surface tension.

In the EHD jet printing system, the critical flow rate (Q_c) and the critical voltage (V_c) interplay with the process conditions (Q_s, V_a) to determine whether the Taylor cone jet is formed or not. Therefore, the processing conditions, Q_c and V_c, can be related through dimensional analysis. Two dimensional processing parameters, dimensionless flow rate (α) and dimensionless voltage (β), is described in Table 3.2.

In this study, we attempted a novel analysis of the processing conditions for the Taylor cone jet formation through the dimensionless variables (α, β), which incorporate the characteristics of the ink and the geometry through the critical flow rate (Q_c) and the critical voltage (V_c).

5.3. Effect of rheological properties

5.3.1. Effect of elasticity

5.3.1.1. Processing window maps

The processing window maps were drawn for all the fluids to visualize the effect of material properties on the formation of Taylor cone jet by changing the flow rate and voltage. Various cone jet modes were captured and classified as the supplied flow rate changed from 0.05, 0.1, 0.3, 0.5, 0.7, 1, 2 to 4 ml/hr. For each flow rate, the voltage was varied from 0 to 15 kV with 0.1 kV increment at a time. The transition boundary of jetting mode was marked with a filled circle on each graph and processing window maps were constructed by connecting these points. All the variables including material properties and processing conditions were presented in terms of the dimensionless numbers for each processing map. The gray zone represents the processing conditions that generate Taylor cone jet.

The processing window maps for the first model system in which only elasticity changes are displayed in Fig. 5.3 and Fig. 5.4. By increasing the polymer relaxation time, the dimensionless number for elasticity, ξ,

increased from 0.09 to 9.93. Other three dimensionless numbers (χ, σ, ε') were kept constant because the physical properties (η, κ, γ, ε') involved in these three dimensionless numbers are almost the same.

The x axis is dimensionless flow rate (α) and y axis is dimensionless voltage(β). The dimensionless initial and final flow rate to form the stable Taylor cone jet was defined as α_i and α_f, respectively. α_i of six model inks(M03-M50) was 1 and α_f of six model inks was the about 40.

Insufficient flow rate produced thin jet and excessive flow rate generated the thick jet. In this system, when thin jet occurred after micro-dripping & intermittent jet due to insufficient flow rate ($\alpha < \alpha_i$). For $\alpha > \alpha_f$, thick jet was observed after micro-dripping & intermittent jet by the flux strength which is the lager than the electric field. When $\alpha_i \le \alpha \le \alpha_f$, Taylor cone jet was observed after micro-dripping & intermittent jet. Since then, tilted, contraction and straight jet appeared in order.

The dimensionless initial and final voltage to form the Taylor cone jet at the each flow rate was defined as β_i and β_f, respectively. Each model system had different cone jet evolution as β increased at the same flow rate. The different cone jet evolution will be explained in term of ξ in the range from α_i to α_f.

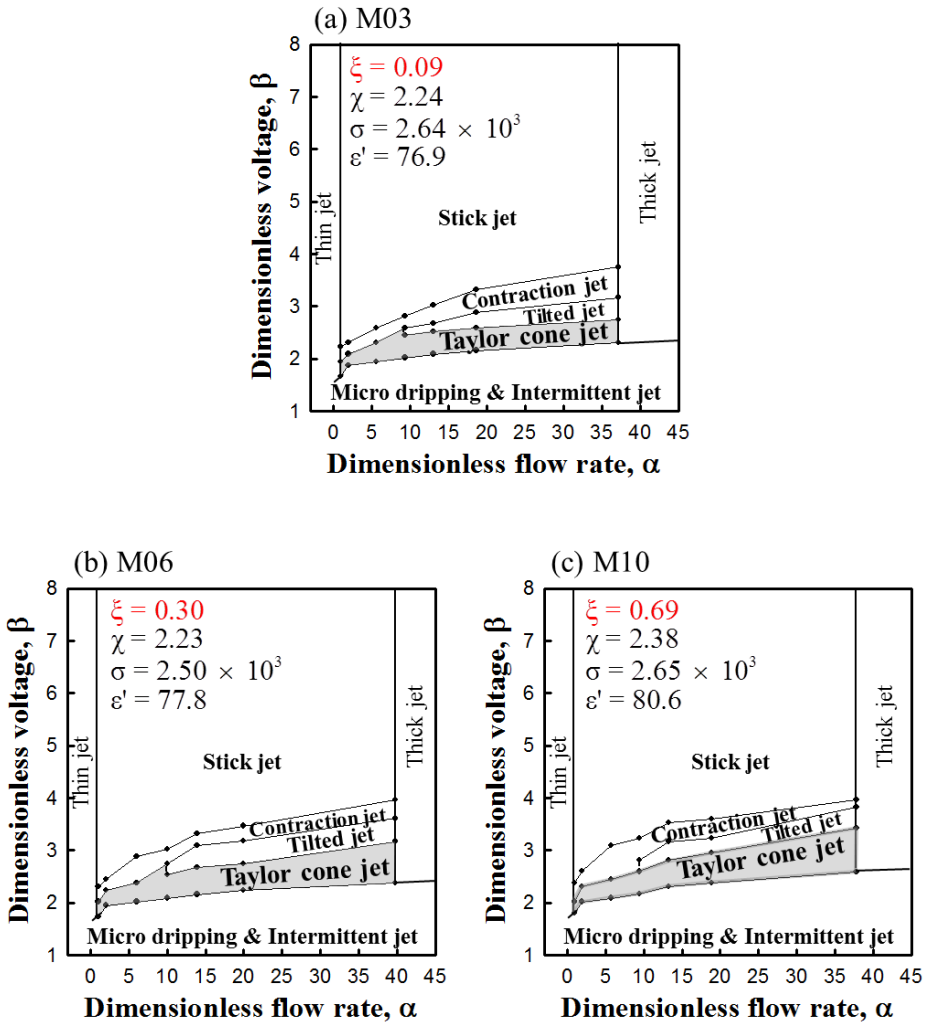

Figure 5.3. Processing window maps for model system Ⅰ with different elasticity: (a) M03, (b) M06, (c) M10.

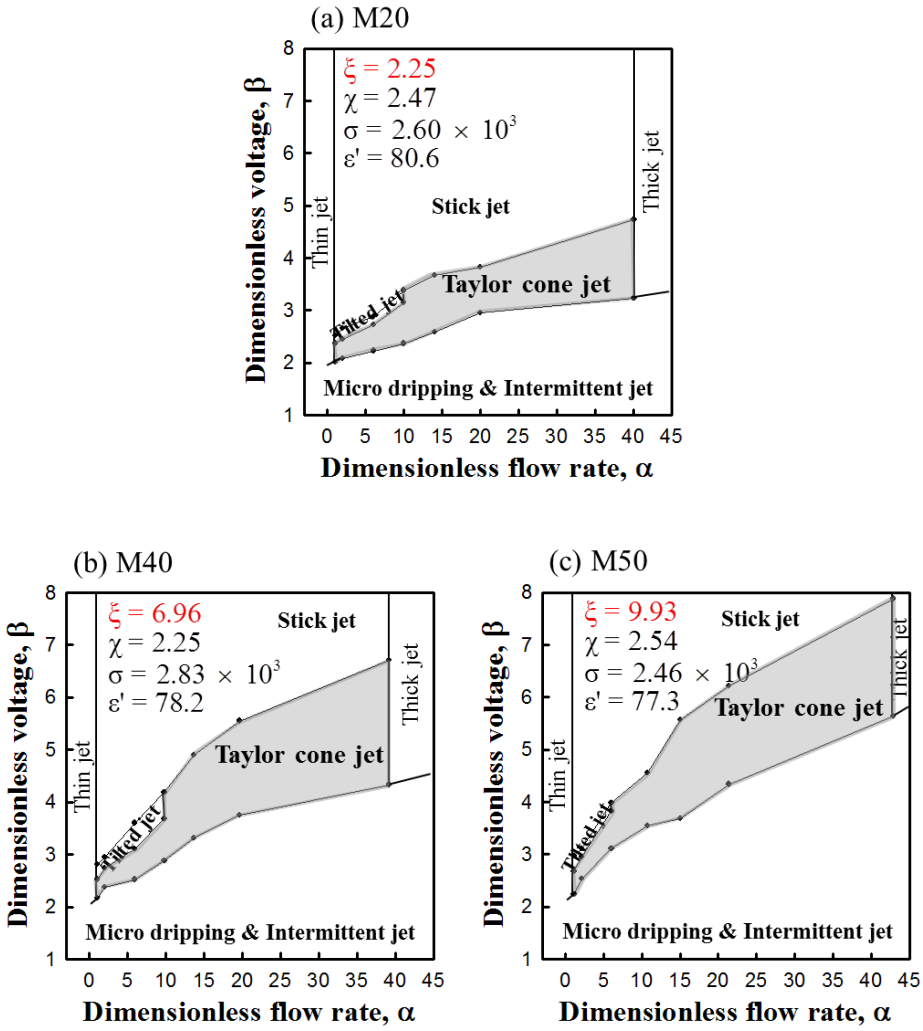

Figure 5.4. Processing window maps for model system Ⅰ with different elasticity: (a) M20, (b) M40, (c) M50.

The range of dimensionless flow rate remains unaffected by increasing the ξ. All inks has similar range of dimensionless flow rate about 1 to 40. On the other hand, the range of β of jetting mode had significant change as ξ increased. The Taylor cone jet zone was shifted by increasing the range of β_i and β_f.

The tendency of the cone jet evolution and the change of the dimensionless voltage range for Taylor cone jet can be classified on the basis of ξ=1. When the ξ was smaller than 1(M03, M06 and M10) as shown in Fig. 5.3, the processing condition for Taylor cone jet and jetting sequence were not significantly changed as function of elasticity of ink. When the ξ was larger than 1 as seen in Fig. 5.4, the processing condition for Taylor cone jet and jetting sequence varied significantly as the elasticity increased.

5.3.1.2. Elasticity parameter, ξ

From the Fig. 5.3 and 5.4, the results demonstrated that the ξ is a key parameter that determines whether elasticity has an effect on the Taylor cone jet formation. The reason why the jetting evolution had different tendency on the basis of $\xi = 1$ is that the jetting system could be dominated by the difference factors when the ξ was smaller or larger than 1.

ξ is defined as the ratio of relaxation time (t_λ) which is proportional to elasticity, to capillary time (t_γ) shown in Eq. 3.4. When $\xi < 1$, the capillary time determines the processing conditions for jetting modes and sequence. The variables (ρ, d, γ) involved in t_γ were fixed. Therefore, when the ξ is smaller than 1, the jetting mode had similar tendency in three model systems (Fig. 5.3). In these conditions, the effect of ink's elasticity reflected in ξ was not significant on the jetting system.

On the other hand, when $\xi > 1$, the elasticity dominated the jetting behavior. Therefore, the elasticity had a dominant effect on the Taylor cone jet formation when $\xi > 1$ while the effect of elasticity was nearly negligible for $\xi < 1$. Especially, the ink's elasticity had a great effect on the range of β of the jetting mode (Fig. 5.4). As ξ increased from 2.25(M20) to 9.93(M50), β_i

was changed the range from 3.24(M20) to 5.64(M50) and β_f was increased the range from 4.32(M20) to 7.88(M50) on the basis of α_f.

In summary, dimensionless number ξ can provide the important information whether the ink's elasticity is dominant factor or not in the jetting system. Furthermore, the results interpret that the ink's elasticity has a close relationship with the rage of β, excluding α.

5.3.1.3. Jet diameter

The jet diameter is an important factor for high resolution patterning as well as the formation of Taylor cone jet. The range of dimensionless voltage to form Taylor cone jet was changed significantly with the increase in elasticity, while the range of the dimensionless flow rate remained the same for all the fluids as seen in Fig. 5.3 and 5.4. We plotted the processing range of dimensionless voltage for the Taylor cone jet formation at the final flow rate α_f as a function of ξ in Fig. 5.5. The gray square was the range of dimensionless voltage for the formation of Taylor cone jet. The lower and upper bounds of gray square were β_i and β_f, respectively.

Fig. 5.5 shows that both β_i and β_f increase with ξ, which implies that elasticity stabilizes Taylor cone jet as well as retards the formation of cone jet. During the increase of ξ from 0.09 to 9.93, the β_f increased from 2.7 to 7.8, which was more than the increase in β_i that ranged from 2.3 to 5.6. Because β_f increased with a higher rate than β_i, the increase of ξ widens the range of β. Therefore, it is concluded that the elasticity has positive effect on the processing conditions in order to form Taylor cone jet.

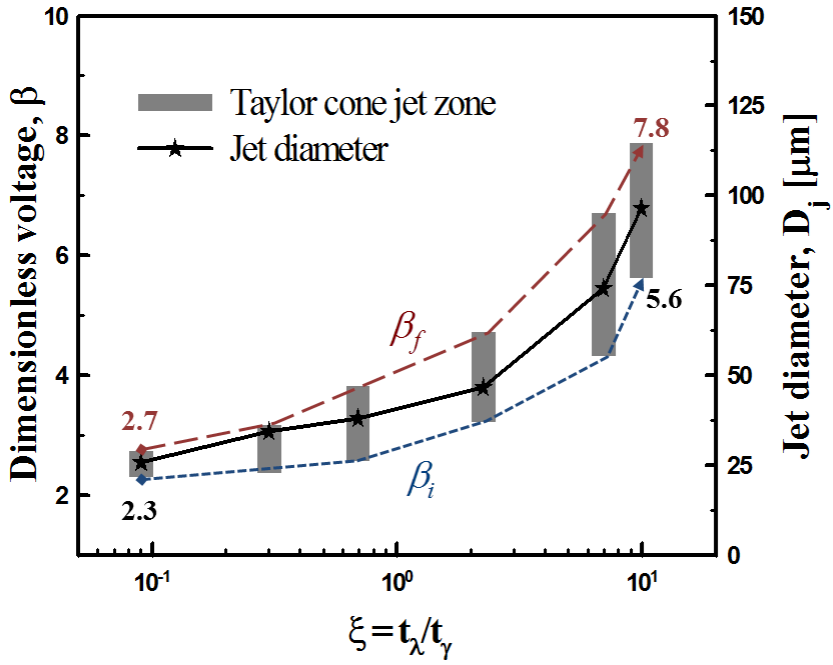

Figure 5.5. Range of the dimensionless voltage for Taylor cone jet and corresponding jet diameter as a function of ξ

Corresponding jet diameters (D_j) at the final flow rate are marked with a star symbol in Fig. 5.5. The jet diameter was measured at the same position - $350\ \mu m$ from the end of the nozzle. The increase of D_j was similar to the increase of dimensionless voltage with the increase in ξ. According to the graph, thick jet ($>100\ \mu m$) could develop for $\xi > 10$. It implies that the ink with high elasticity may produce thick jet if it is too elastic ($\xi > 9.93$) although the elasticity widens the processing window for Taylor cone jet. Therefore, the jet diameter should be considered simultaneously to obtain high resolution patterns even though the elasticity enhances the accessible range of Taylor cone jet.

5.3.2. Effect of viscosity

5.3.2.1. Processing window maps

The effect of viscosity on the jetting mode was investigated by drawing the processing window map for the fluids of model system Ⅱ where only the viscosity was varied as in Fig. 5.6 and 5.7. The dimensionless number χ was increased from 0.74 to 2.96 as the ink viscosity changed from 9.5 to 36.9 cp. Other three dimensionless numbers (ξ, σ, ε') were almost the same because the physical properties (λ, κ, γ, ε') involved in these dimensionless numbers were kept constant. The values of ξ, χ, σ, ε' were given in the upper left of each graph.

Various jetting modes were observed in the range of α_i to α_f. The values of α_i and α_f were different depending on the physical properties of the inks. Jetting sequence for all the fluids contained in this model system followed the typical jet evolution of viscoelastic fluids mentioned in the previous section.

Taylor cone jet zone was widened as the viscosity increased. Fig. 5.6 and 5.7 show the different tendency of cone jet evolution on the basis of χ=1.

When $\chi < 1$ (Fig. 5.6), the Taylor cone jet zone was narrow, and unstable jets such as thin and thick jet appeared in a wide range of processing conditions due to insufficient or excessive flow rate, and the viscosity did not influence the stability of Taylor cone jet significantly. Under this condition, the increase in viscosity widened the range of α for the formation of Taylor cone jet, which implies that the viscosity acts as a resistance against the instability of the jet caused by the flow rate. In general, $\alpha = 1$ has been considered as a critical point where the supplied flow rate satisfies the critical flow rate and Taylor cone jet formation [Lee et al. (2013)]. However, two model inks in this study did not form Taylor cone jet at $\alpha = 1$ as seen in Fig. 5.6a (C18) and 5.6b (C24). This result indicates that the viscosity is not enough to maintain the stable cone jet regardless of the processing conditions.

When the effect of viscosity was predominant over other properties ($\chi > 1$), the increase of viscosity widened the range of voltage for the Taylor cone jet by increasing the β_f while minimally affecting the β_i as seen in Fig. 5.7.

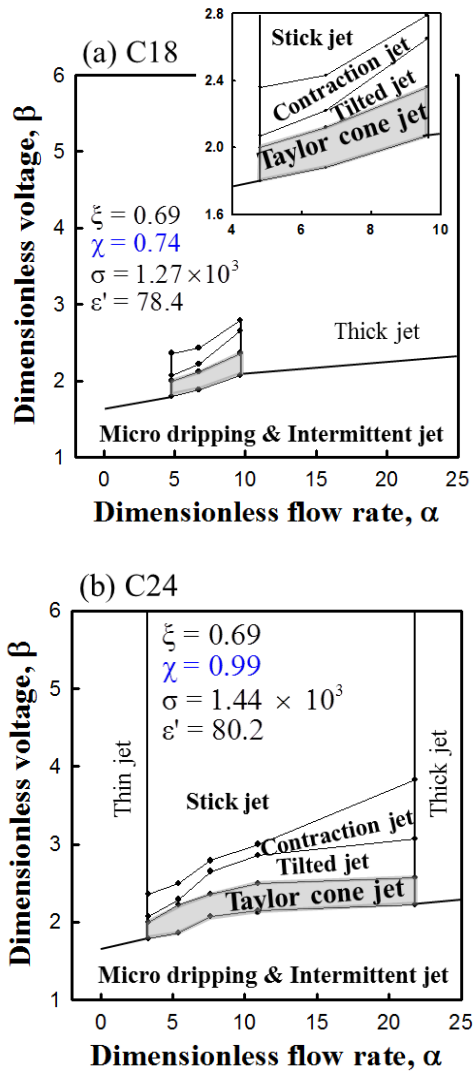

Figure 5.6. Processing window maps for Model system Ⅱ: (a) C18, (b) C24.

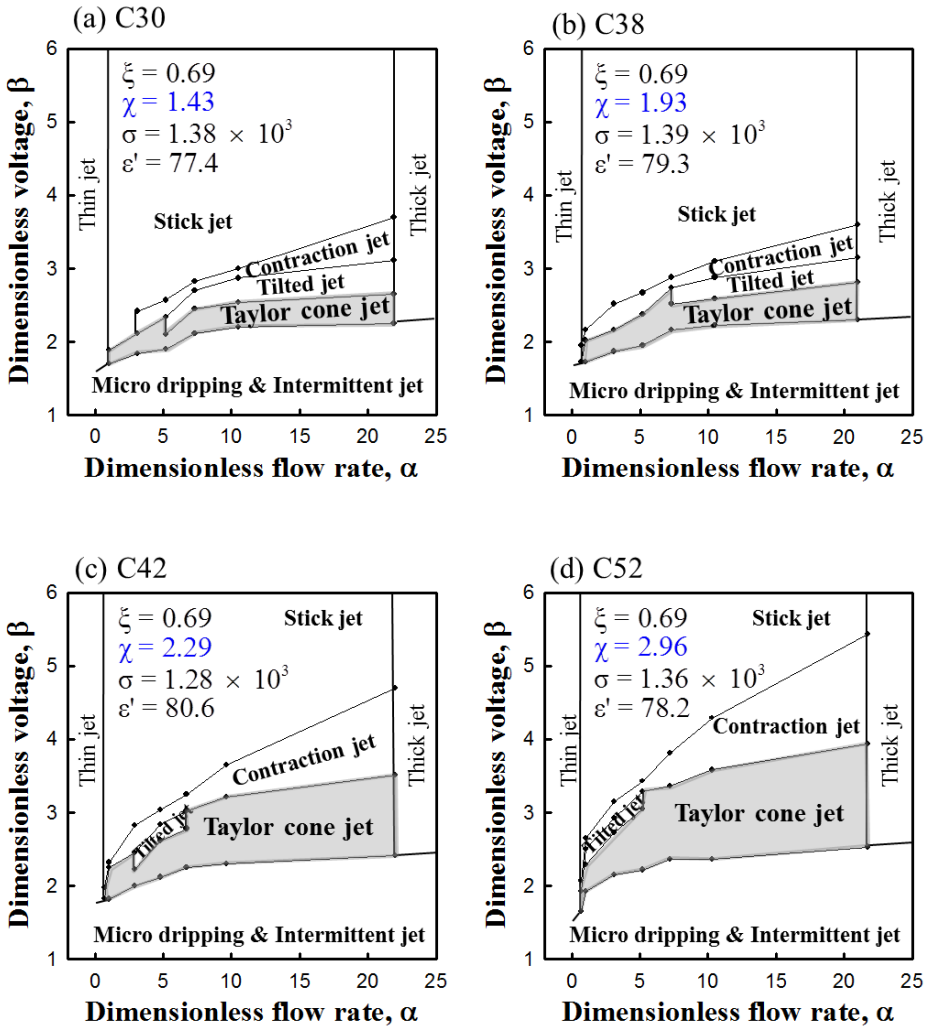

Figure 5.7. Processing window maps for Model system Ⅱ: (a) C30, (b) C38, (c) C42, (d) C52.

5.3.2.2. Viscosity parameter, χ

From the analysis of processing window maps for model system Ⅱ (Fig. 5.6 and 5.7), we can know that the Taylor cone jet zone was influenced mainly by different processing condition on the basis of $\chi=1$. It is related to the definition of χ which is consisted of two characteristic velocity: propagation velocity of perturbation ($\eta/\rho d$) and characteristic velocity of fluid (Q_c/d^2) (see Eq. 3.5).

For the case of $\chi<1$, characteristic velocity of fluid was dominant factor in jetting system than propagation velocity of perturbation. In this condition as seen in Fig. 5.6, even though sufficient flow rate was supplied, cone jet couldn't form and had a narrow processing condition for cone jet.

For the case of $\chi>1$, propagation velocity of perturbation was dominant factor in jetting system than characteristic velocity of fluid. For this condition as seen in Fig. 5.7, cone jet was formed even though insufficient flow rate was supplied ($\alpha<1$).The results obtained in our experiment indicate that the role of the ink's viscosity resisting fluid velocity is important to form and maintain the cone jet formation especially in the initial condition of α.

In addition, when the χ was larger than 1, the Taylor cone jet zone widen not only the range of α but also the range of β_f as χ increased. As

viscosity increased from C30(χ =1.43) to C52(χ =2.96), β_i had similar value about 2.3 but β_f increased the range from 2.65 to 3.93. The increase of β_f means that the viscosity has an effect on the stability of Taylor cone jet to maintain more longer after forming cone jet.

Therefore, χ is larger than 1 is the necessary condition to form the stable cone jet for the ink of EHD jet printing. The ink having high viscosity widens the stable cone jet zone.

5.3.3. Forces exerted on the surface of Taylor cone jet

5.3.3.1. Forces

The shape of Taylor cone is preserved when the normal ($F_{E,n}$) and tangential ($F_{E,t}$) components of electric stress generated by electric potential (F_E) are balanced with the fluid properties on surface. The normal stress ($F_{E,n}$) acts to the outward direction onto surface, balancing with inward direction of normal stress such as surface tension. Upon reaching this balance, fluid moves down to the cone apex by tangential component of electric stress ($F_{E,t}$), resulting in Taylor cone shape as shown in Fig. 5.8.

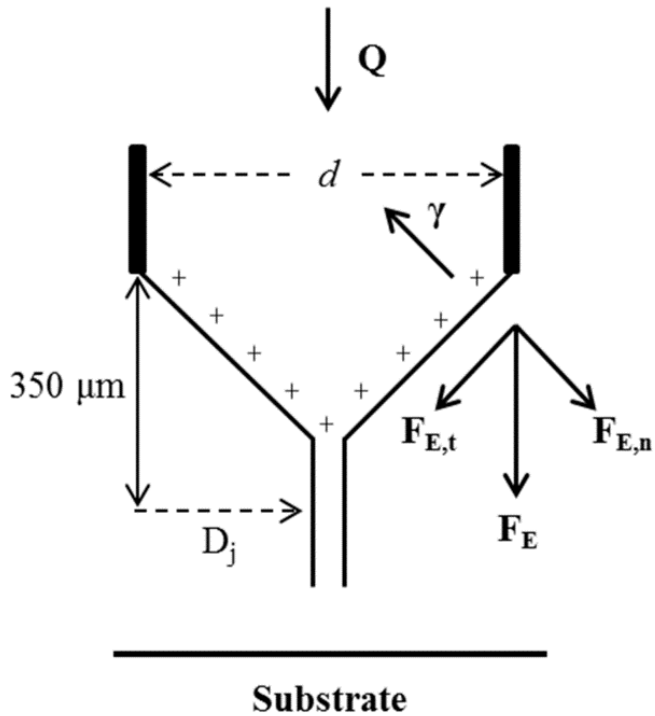

Figure 5.8. The schematic of force exerted on the surface of Taylor cone

5.3.3.2. The role of elasticity

The processing window maps (Fig. 5.4) show that the Taylor cone jet zone was widened as the elasticity of the ink increased. The increase of elasticity widened the range of voltage by increasing the β_f more than β_i, while the range of the flow rate for Taylor cone jet stayed independent of elasticity. This result can be confirmed when the effect of elasticity is analyzed in terms of the relationship between the stresses acting on the surface of the Taylor cone jet as seen in Fig 5.8.

β_i increased as elasticity increased as shown in Fig. 5.4, which indicates that a higher electric potential is required to be balanced with inward direction of normal stress. This result demonstrated that elasticity enhanced the required normal stress to form the Taylor cone jet by acting on the opposite direction to the normal stress, i.e, the same direction as the surface tension. Therefore, elastic stress stabilizes the drop and retards the formation of Taylor cone jet.

The increase of elasticity also induces the increase in β_f (Fig. 5.4), which is defined as the voltage at the transition point from Taylor cone jet to unstable jet. In this system, the breakup of Taylor cone jet is a result of the competition between the normal and tangential stress because the material properties are maintained to be constant [Hartman et al. (1999), (2000)]. Therefore, the

increase in β_f implies that Taylor cone jet is stable over a large range of voltage as the balance between the normal and the tangential stress is maintained even at higher electric potentials. It is because Taylor cone jet in elastic fluid is initially formed at large normal stress. On the other hand, Newtonian fluids have much smaller β_i, as they have no elasticity. The balance between the normal and tangential stress is easily broken with a small increase in the electric potential and low β_f is observed [Lee et al. (2013)]. Thus, it can be concluded that even though elasticity retards the formation of Taylor cone jet, it improves the stability of the conical shape of the jet.

The elastic effect invokes another important characteristic in jetting behavior such that the Taylor cone jet changes directly to stick jet without going through contraction jet stage as seen in Fig. 5.4. In the case of a Newtonian fluid, twin or multi- jets occur at the excessive voltage that causes the increase in the normal component of electric stress [Lee et al. (2013)]. However, in the case of a viscoelastic fluid, the tangential component of electric stress increases as the elastic stress shields the effect of the normal stress. The increase in tangential stress causes the cone to thin rapidly by accelerating the charges on the surface towards the cone apex [Taylor & Francis group (2009), Hartman et al. (2000)]. Therefore, the Taylor cone jet changes immediately to stick jet under an excessive electric potential.

5.3.3.3. The role of viscosity

The role of viscosity on Taylor cone jet can be deduced from the analysis of the stresses acting on the surface of the liquid.

As shown in Fig. 5.7, the β_i did not vary significantly with the increasing viscosity. Because the β_i was determined when the normal component of electric stress was balanced with the inward direction of normal stress, this data demonstrated that viscosity did not exert stress to the normal direction of the Taylor cone jet surface. On the other hand, the β_f increased with increasing the viscosity, which means that the tangential stress kept balancing with normal electric stress even though the electric potential increased. Because the normal electric stress was maintained to be constant, the increase of β_f with the increasing viscosity indicated that viscosity prevented the increase of tangential component of the stresses. It is implied that the viscosity generates stress in the opposite direction of the tangential electric stress. Therefore, viscosity stabilizes Taylor cone jet by resisting the effect of tangential electric stress.

5.4. Effect of electrical property depending on rheological properties

5.4.1. Effect of conductivity

In order to observe how the electrical conductivity affects the Taylor cone jet formation, the jetting shapes of the five inks of model system Ⅲ-1 were observed using a high-speed camera at flow rates $0.07-4.0\ ml/hr$ and at voltages increasing with an increment $0.1\ kV$. In Fig. 5.9, the processing conditions for Taylor cone jet of two inks (M10K20 and M10K100) of model system Ⅲ-1 with the largest conductivity difference are provided.

We defined the minimum supplied flow rate for the formation of Taylor cone jet as the initial flow rate (Q_i) and the maximum supplied flow rate as the final flow rate (Q_f). Below the initial flow rate or above the final flow rate, Taylor cone jet did not form regardless of the applied voltage. The filled triangles correspond to the lowest applied voltages at which the Taylor cone jets are formed, and they are defined as the initial voltage (V_i). The open triangles correspond to the highest applied voltage where the Taylor cone jets are formed at each flow rate and are named as the final voltage (V_f). In other words, the voltages from V_i to V_f correspond to the range of the voltages

in which the Taylor cone jet is observed. The Taylor cone jet zone is depicted in Fig. 5.9 by gray color.

As the ink's conductivity increased from 20 to 100 $\mu S / cm$, both the final flow rate and the flow rate range decreased. At the same flow rate, the increase of conductivity resulted in the increase of initial and final voltages. This resulted in the Taylor cone jet zone existing at high voltage range for highly conductive inks.

In order to observe how the Taylor cone jet zone changes depending on the conductivity, we plotted the flow rate range (Q_i, Q_f) and the voltage range (V_i, V_f) of the five inks of model system Ⅲ-1 in Fig. 5.10.

Fig. 5.10a shows the flow rate range for Taylor cone jet formation depending on the conductivity. As the conductivity increased, the flow rate range slightly decreased. The initial flow rate was around $0.07-0.5\ ml/hr$ and the increase of conductivity did not significantly alter the initial flow rate. As the conductivity increased, the final flow rate decreased. Thus, the change in the range of flow rate arises due to the change in the final flow rate. Two different types of unstable jets were observed above the final flow rate. First is the thick jet that occurs when the jet becomes as thick as the nozzle size due to the high flow rate. Another is the tilted or contraction jet that occurs as the high voltage tilted the direction of the jet or contracted the conical shape.

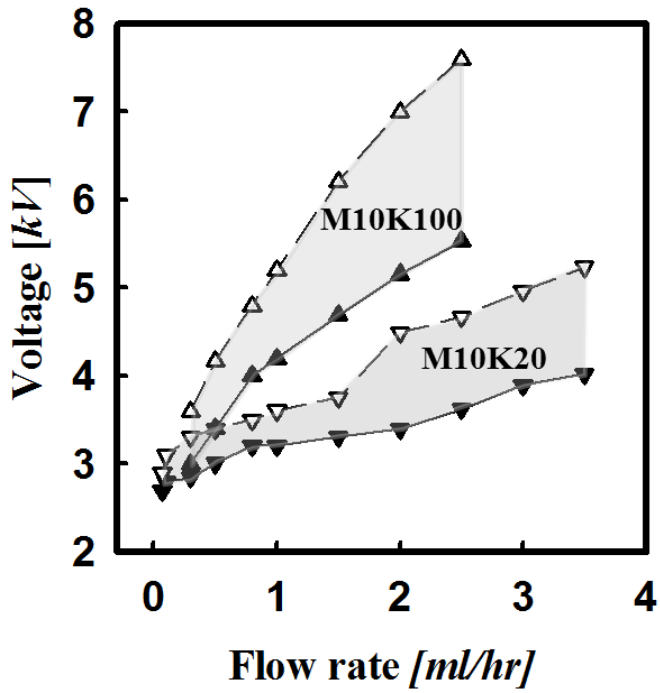

Figure 5.9. Processing conditions (gray regions) of Taylor cone jet for PEO solutions with different electrical conductivity; filled triangles for initial voltage (V_i) and open triangles for the final voltage (V_f).

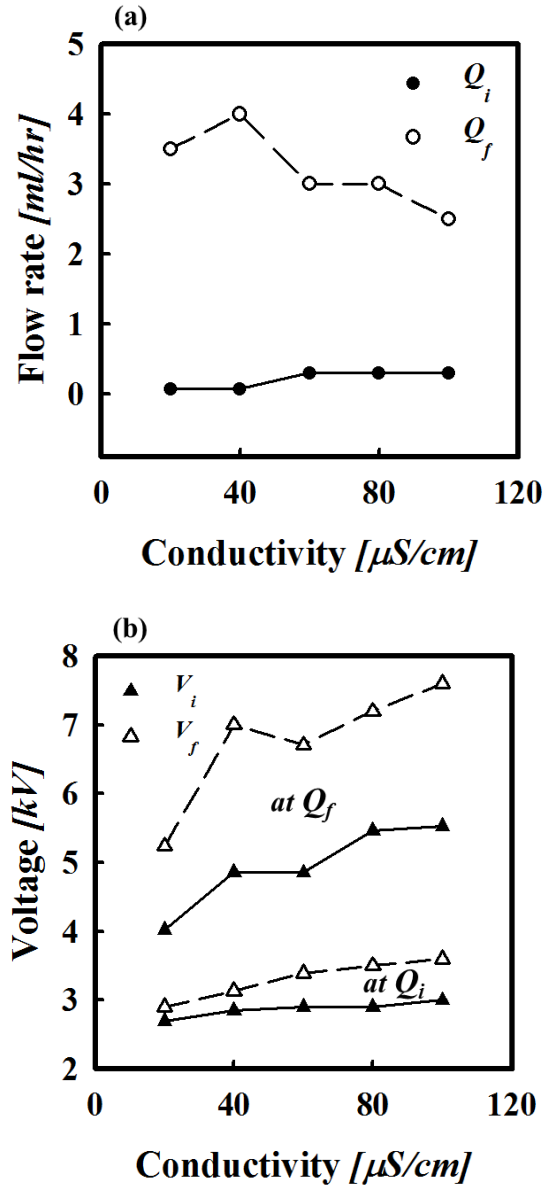

Figure 5.10. Flow rate range (a) and voltage range (b) of Taylor cone jet zone as a function of electrical conductivity for model system Ⅲ-1

To analyze the change in the range of voltage for the Taylor cone jet formation caused by the increase in the electrical conductivity, we plotted the initial and final voltage for both the initial and final flow rates as a function of ink conductivity in Fig. 5.10b. The increase in conductivity resulted in the rise of both the initial and final voltage, and the Taylor cone jet zone was located at higher voltages. The increase in electrical conductivity is known to facilitate the formation of the conical shape because the transport of the charges to the ink surface becomes more rapid due to the decrease of charge relaxation time ($t_c = \varepsilon' \varepsilon_o / \kappa$) [Mora (2007), Stanger et al. (2009)]. However, this theory applies only when the surface area of the conical shape is comparable. In previous research, the initial voltage was increased when the electrical conductivity became larger, as the surface area of the initially formed conical shape increased and the accumulation of more charges became necessary [Carroll et al. (2006)]. The samples in our study also exhibited the same trend of the increase of initial voltage with the increase of electrical conductivity. The Taylor cone jet first formed at the initial voltage and maintained its conical shape until the final voltage. After the final voltage, unstable jet was observed. The increase of the final voltage at larger electrical conductivity signifies that the electrical conductivity increases the stability of the conical shape at high voltages.

5.4.2. Effect of conductivity depending on the viscoelasticity

In order to examine the role of electrical conductivity for the inks of different rheological properties, we analyzed the Taylor cone jet zone for model system Ⅲ-2 and Ⅲ-3 which have different elasticity and viscosity when compared with the model system Ⅲ-1. The comparison of model system Ⅲ-1 and Ⅲ-2 reveals the role of elasticity on the effect of conductivity while the difference in model system Ⅲ-1 and Ⅲ-3 demonstrates the role of viscosity on the conductivity. For this purpose, we provide the flow rate and voltage ranges for the Taylor cone jet zone of all three model systems in Fig. 5.11 and 5.12, respectively.

Fig. 5.11 shows the flow rate range for Taylor cone jet formation of the three model systems. The initial flow rates were not affected by the conductivity regardless of the inks' viscoelasticity. The final flow rates for the high viscosity case (model system Ⅲ-3) decayed similar to the model system Ⅲ-1 as the conductivity increased, while the final flow rates for the high elasticity case (model system Ⅲ-2) did not exhibit any conductivity dependence.

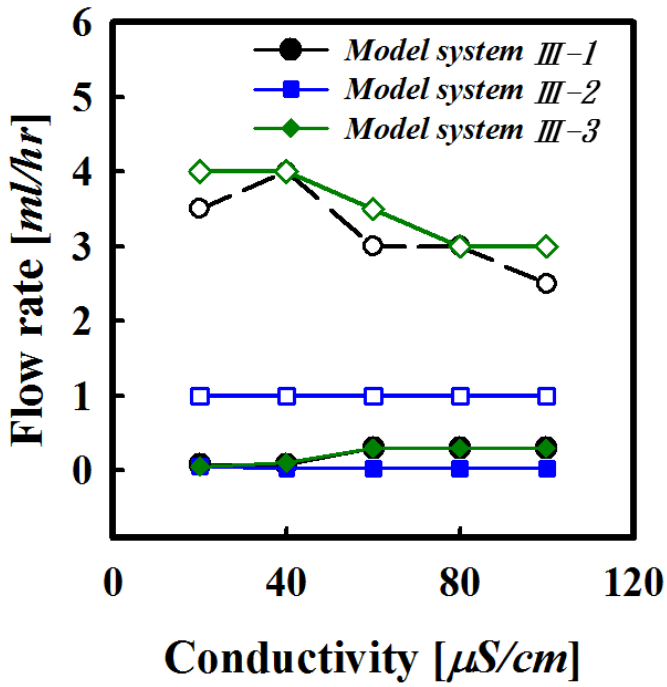

Figure 5.11. Flow rate range for Taylor cone jet formation as a function of electrical conductivity for model systems Ⅲ-1, 2, and 3; filled symbols for the initial and open symbols for the final flow rate

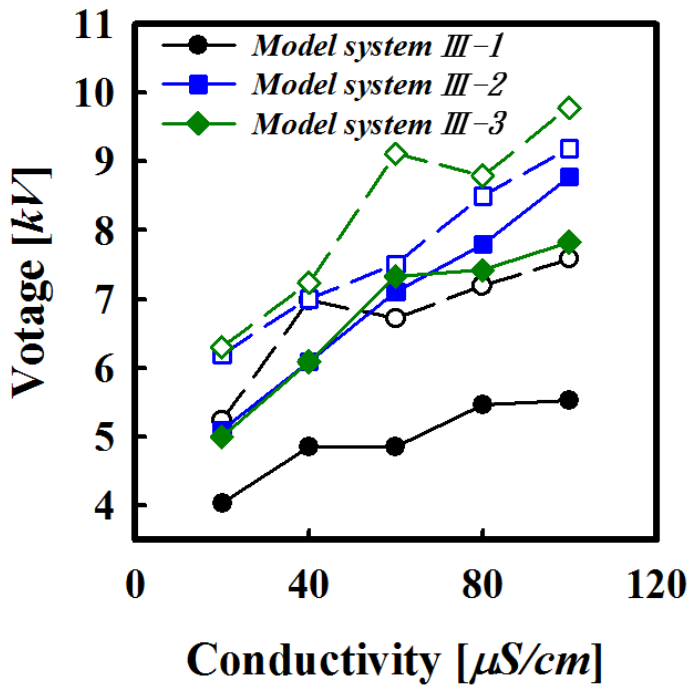

Figure 5.12. Voltage range at final flow rate for Taylor cone jet formation as a function of electrical conductivity for model systems Ⅲ-1, 2, and 3; filled symbols for the initial and open symbols for the final voltage

The voltage ranges for the Taylor cone jet were also observed. To compare the voltage ranges at the same flow condition, the initial and final voltages at the final flow rates of each system are plotted as a function of conductivity in Fig. 5.12. The initial and final voltage increased with the increase in electrical conductivity for the three model systems. The reason that the voltage range increases with electrical conductivity was explained in section 5.4.1. From Fig. 5.10b, we can say that the electrical conductivity plays the same role even in the rheologically different inks.

One important issue is the role of the interaction between the electrical conductivity and the viscoelasticity of the ink on the Taylor cone jet formation. By observing the change in the initial and final voltages of model systems Ⅲ-1, 2 and 3 when the conductivity increases from $20 \text{ to } 100\ \mu S/cm$, we can analyze the effect of conductivity depending on the rheological properties of the inks (Fig. 5.12). If the voltage range of the Taylor cone jet is affected solely by the electrical conductivity regardless of the viscoelastic properties of the inks, all the model systems Ⅲ-1, 2 and 3 should have the same rate of increase in voltage as the conductivity increases. However, as shown in Fig. 5.12, the voltages of the inks with larger elasticity and viscosity (model system Ⅲ-2 and 3) increased more steeply in response to the increase of the electrical conductivity than the model system Ⅲ-1. From the larger initial voltages for

model systems Ⅲ-2 and 3, it can be postulated that the increased viscoelasticity required larger voltage to transport and accumulate charges on the surface for the Taylor cone jet formation. If we consider only the electrical property, we may expect that the transport mobility of the charge is the same for all the systems as the charge relaxation time is the same. However, it's now clear that the inks' rheological properties influence the transport mobility of the charge too. In summary, the effect of the electrical conductivity on the Taylor cone jet formation is most pronounced in the model system Ⅲ-1, and is reduced as the viscoelasticity of the ink increases the initial voltage by obstructing the charge transport to the surface of conical shape (charge conduction).

In order to keep Taylor cone jet after its formation, the amount of charge on the conical surface of the jet needs to be maintained. Thus, rather than comparing the effect of conductivity only on the final voltages, the ranges of voltages need to be considered too. The results from model system Ⅲ-1 demonstrated that the inks with larger conductivity maintained the Taylor cone jets at wider ranges of the voltages (Fig. 5.10b). In Fig. 5.12, the voltage range decreased significantly for the more elastic model system Ⅲ-2 and decreased slightly for the more viscous model system Ⅲ-3. These results indicate that the unstable jets are formed more easily in more viscoelastic inks. The jet

stabilizing effect of the electrical property is more pronounced for the ink with less viscoelasticity, indicating that the viscoelasticity obstructs the stabilizing effect of the electrical conductivity.

Even with the same amount of increase in the electrical conductivity, the increase of the initial voltages was larger for more elastic (model system Ⅲ-2) and viscous (model system Ⅲ-3) inks than the model system Ⅲ-1 because the charge transport was more slow. In addition, more viscoelastic inks had narrower voltage ranges than the model system Ⅲ-1. This also demonstrates that the viscoelasticity reduces the stabilizing effect of the electrical conductivity on the Taylor cone jet formation.

Consequently, while the electrical conductivity and the rheological properties affect the jetting process with different mechanisms, both properties increase the initial and final voltages for Taylor cone jet formation.

5.4.3. Processing window maps

The processing window map of model system Ⅲ-1, described by the dimensionless flow rate (α) and dimensionless voltage (β), is shown in Fig. 5.13. The processing conditions for the Taylor cone jet are marked by gray zones to distinguish them from the unstable jetting conditions (micro-dripping, tilted, contraction, stick, thin and thick jets). We focus on the processing conditions for Taylor cone jet formation.

From Fig. 5.13, the biggest change according to the increase in conductivity is the shift of the dimensionless flow rate region for the Taylor cone jet zone. For 20 $\mu S/cm$ ink (M10K20), the dimensionless flow rate range for the Taylor cone jet formation was $1<\alpha<60$ (M10K60), while the flow rate range was $14<\alpha<140$ for 60 $\mu S/cm$ ink. For 100 $\mu S/cm$ ink (M10K100), the flow rate range was $25<\alpha<210$ for the Taylor cone jet zone.

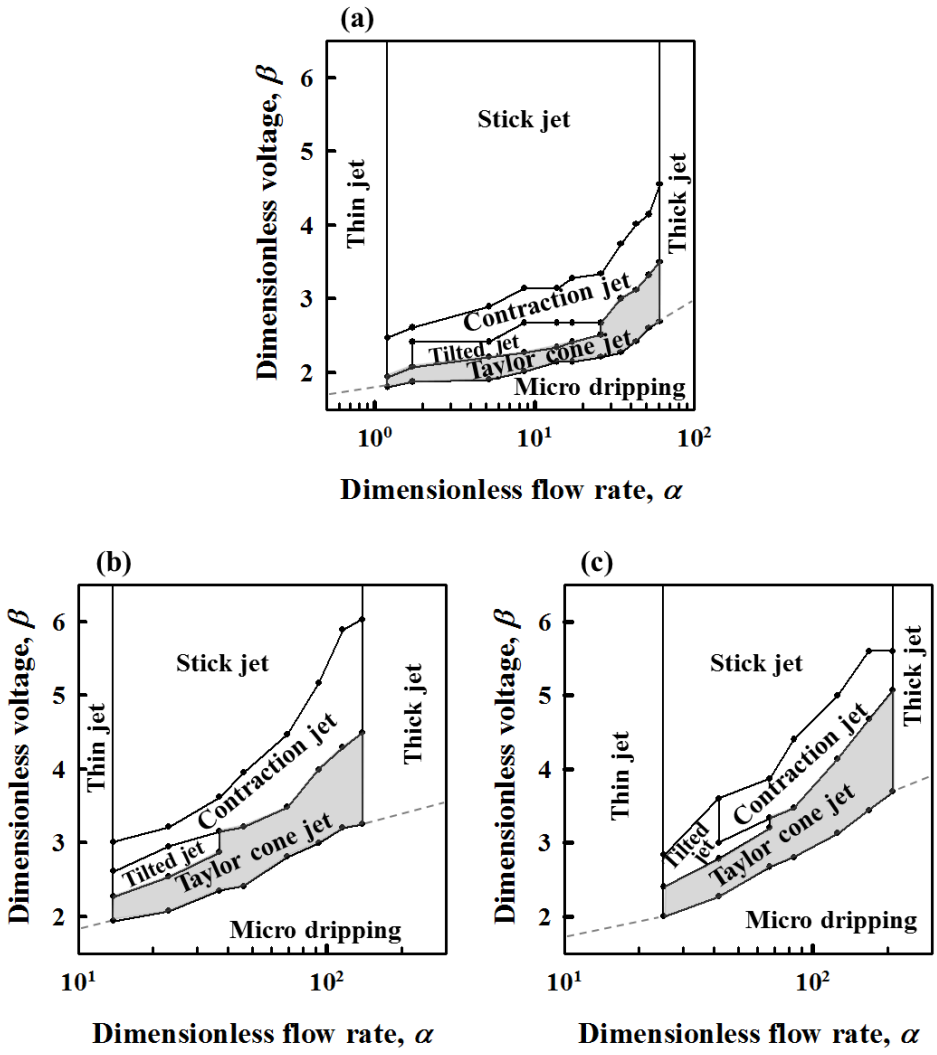

Figure 5.13. Processing window maps for model system Ⅲ-1: (a) M10K20, (b) M10K60, (c) M10K100.

The increase of the dimensionless flow rate (α) to form the Taylor cone jet with the increase in conductivity is related to the $Q_s/Q_c = \rho\kappa Q_s/\varepsilon_o\varepsilon^{'}\gamma$ in which the dimensionless flow rate involves the electrical conductivity. Dimensionless flow rate reflects the interaction between experimentally supplied flow rate and the specific flow rate which is caused by the flow of the charge on the Taylor cone jet surface towards the apex direction due to the applied voltage. The specific flow rate is influenced by the charge relaxation time which determines the transport mobility of the charges to the fluid surface [Zong et al. (2002), Lim et al. (2011)].

In summary, the increase of electrical conductivity causes a decrease of the charge relaxation time which results in an increase of the specific flow rate and consequently an increase of α .

5.4.4. Interplay between the conductivity and the viscoelasticity

The processing window map of Fig. 5.13 revealed that the dimensionless flow rate range increased with the increase in conductivity. In order to see the change in Taylor cone jet zone, we depicted the processing window maps for all of the inks of model system Ⅲ-1, 2 and 3 which have different rheological properties in Fig. 5.14, 5.15 and 5.16, respectively.

As can be observed in Fig. 5.14, the Taylor cone jet zone for 20 $\mu S/cm$ ink was in between $1<\alpha<60$. As the conductivity increased to 40 $\mu S/cm$, the range of α increased to $2<\alpha<130$ and the Taylor cone jet zone shifted toward the right side of the graph. This trend of the increase of α range with the increase in conductivity was observed for all the inks. Interestingly, all of the inks exhibited similar β_i and β_f at the same α, and the β_i and β_f of the inks of model system Ⅲ-1 formed a single master curve with respect to the dimensionless flow rate (α). In the model systems Ⅲ-2 (Fig. 5.15) and Ⅲ-3 (Fig. 5.16), the single master curve with respect α was also observed.

The electrical conductivity has an influence on the charge relaxation time, which determines the specific flow rate. The interaction between specific

flow rate and experimentally supplied flow rate is reflected in the dimensionless flow rate. Thus, the value of β_i and β_f as a function of dimensionless flow rate (α) reflects the role of the interplay between the electrical conductivity and the viscoelasticity of the ink and determines the processing conditions of Taylor cone jet zone.

The β_i and β_f were larger for more elastic ink (comparing model systems Ⅲ-1 and 2) at the same α, and the β_i and β_f both increased for more viscous ink (comparing model systems Ⅲ-1 and 3). This is because more elastic or viscous inks have larger initial and final voltages by obstructing the effect of conductivity, as reported previously in section 5.4.2 (Fig. 5.12).

By constructing the processing window maps ($\alpha - \beta$ graph) of the three model systems, the effect of both the electrical and rheological properties on the Taylor cone jet zone was observed, which could be interpreted as the effect of the interplay between the electrical properties and the rheological properties on the Taylor cone jet.

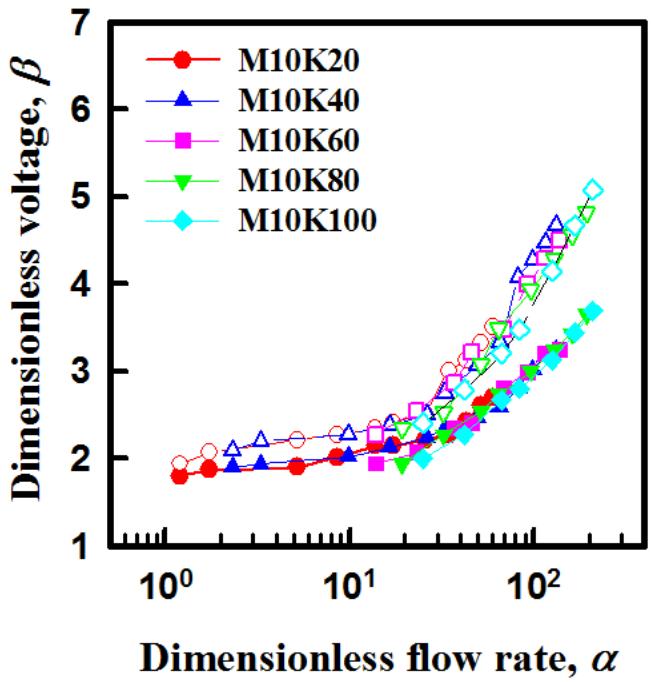

Figure 5.14. Model system Ⅲ-1. Dimensionless initial (filled symbol) and final voltage (open symbol) of Taylor cone jet formation as a function of dimensionless flow rate

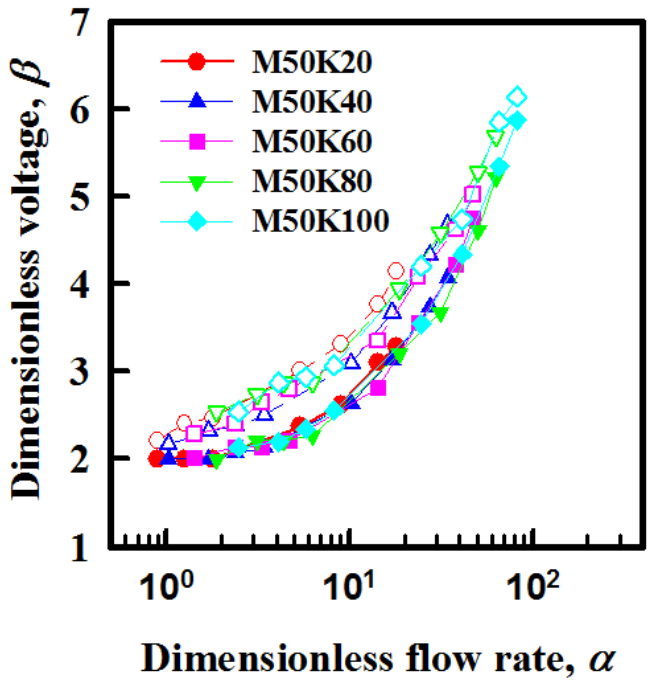

Figure 5.15. Model system Ⅲ-2. Dimensionless initial (filled symbol) and final voltage (open symbol) of Taylor cone jet formation as a function of dimensionless flow rate

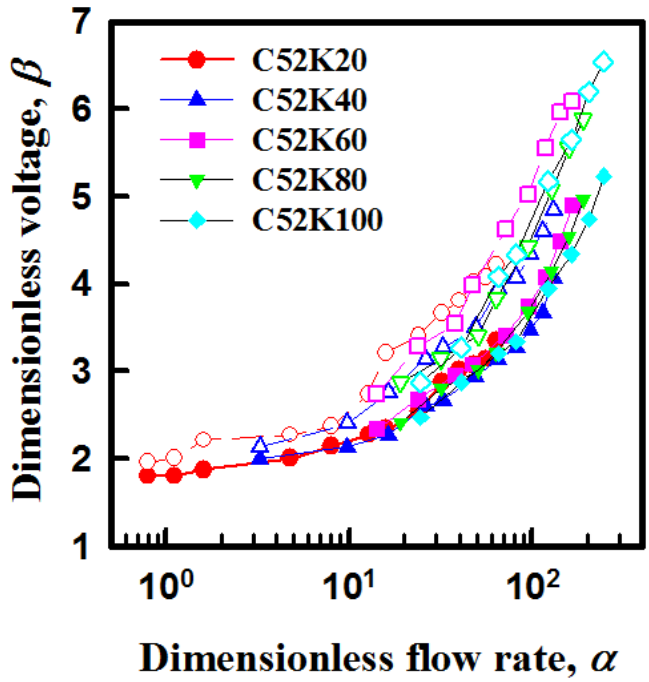

Figure 5.16. Model system Ⅲ-3. Dimensionless initial (filled symbol) and final voltage (open symbol) of Taylor cone jet formation as a function of dimensionless flow rate

Chapter 6.

Summary

In this study, viscoelastic inks and processing conditions were optimized by utilizing well-defined model systems and dimensionless parameter affected to EHD jet printing. First, the effect of viscoelasticity on the formation of Taylor cone jet has been investigated by designing two model inks in which the elasticity and viscosity are controlled separately. The Taylor cone jet zone was widened as both elasticity and viscosity increase in each model system, and they had significant influences on the Taylor cone jet formation when both dimensionless numbers ξ and χ were larger than 1. In the model system in which only elasticity is changed, the increase of elasticity widened the Taylor cone jet zone by increasing β_f more than the increase in β_i, indicating that elasticity retarded both breakup and formation of Taylor cone jet. In the model system in which only viscosity was changed, the viscosity widened the processing range of α for $\chi < 1$, while it increased the processing range of β_f for $\chi > 1$. Although both elasticity and viscosity increase the stability of Taylor cone jet, too high elasticity or viscosity should be avoided because the jet diameter is being increased from viscoelasticity, which may induce thick jet that is not suitable to produce high resolution patterns.

Secondly, the interaction between the electrical and rheological properties of the inks on the formation of the Taylor cone jet was examined. With the different inks of model system Ⅲ-1, which have the same rheological

properties but different electrical properties, we found that the inks with high electrical conductivity form the jets of conical shape with large surface area. This resulted in larger initial voltage for the Taylor cone jet formation as the large surface required more transport of charges on the surface. After forming the Taylor cone jet, the inks with high conductivity maintained the conical shape up to high voltage by raising the stability of the meniscus. Consequently, the final voltages increased with the increase in conductivity. The inks with larger elasticity (model system Ⅲ-2) or viscosity (model system Ⅲ-3) when compared with model system Ⅲ-1 exhibited increased initial and final voltages, which is caused by obstructing the role of the electrical conductivity on the stability of Taylor cone jet. While the electrical conductivity and the rheological properties affect the jetting process with different mechanisms, their influence on the Taylor cone jet zone was similar. In addition, the processing window maps were organized through two dimensionless process variables, dimensionless flow rate (α) and dimensionless voltage (β), which incorporate all the ink properties. The change of processing window maps according to change of the material properties of the ink clearly showed the effect of the interplay between the electrical properties and the rheological properties on the Taylor cone jet formation. The method of dimensional

analysis was found to yield a useful tool for predicting the Taylor cone jet zone for the inks of various electrical and rheological properties.

This study provides the guideline for determining the optimum properties of the printing ink and the processing conditions to obtain the ideal jetting mode in EHD jet printing process.

Bibliography

In alphabetical order by first author,

Angammana, C. J.; Jayaram, S. H. Analysis of the effect of solution conductivity on electrospinning process and fiber morphology. *IEEE. T. Ind. Appl.* **2011**, *47*, 1109-1117.

Barrero, A.; Ganan-Calvo, A. M.; Davila, J.; Palacios, A.; Gomez-Gonzalez, E. The role of the Electrical conductivity and viscosity on the motions inside Taylor cones. *J. Electrost*. **1999**, *47*, 13-26.

Bober, D. B.; Chen, C. -H. Pulsating electrohydrodynamic cone-jets: from choked jet to oscillating cone. *J. Fluid Mech*. **2011**, *689*, 552-563.

Brown, N. A.; Gladstone, J. N.; Chiarot, P. R. Evolution of nanoparticle deposits printed using electrospray. J. Micro. Nano-Manuf. 2015, 3, 014502

Carroll, C.; Joo, Y. L. Electrospinning of viscoelastic Boger fluids: modeling and experiments. *Phys. Fluids* **2006**, *18*, 053102.

Carroll, C. P.; Joo, Y. L. Axisymmetric instabilities in electrospinning of highly conducting, viscoelastic polymer solutions. *J. Non-Newtonian Fluid Mech.* **2008**, *153*, 130-148.

Chen, D. –R.; Pui, D. H.; Experimental investigation of scaling laws for electrospraying: dielectric constant effect. *Aerosol Sci. Technol*. **1997**, *27*, 367-380.

Chen, X.; Jia, L.; Yin, X.; Cheng, J.; Lu, J. Spraying modes in coaxial jet electrospray with outer driving liquid. *Phys. Fluids* **2005**, *17*, 032101.

Choi, K. -H.; Duraisamy, N.; Muhammad, N. M.; Kim, I.; Choi, H.; Jo, J. Structural and optical properties of electohydrodynamically atomized TiO_2 nanostructured thin films. *Appl. Phys. A* **2012**, *107*, 715-722

Cloupeau, M.; Prunet-Foch, B. Electrohydrodynamic spraying functioning modes: a critical review. *J. Aerosol Sci.* **1994**, *25*, 1021-1036

Conroy, D. T.; Matar, O. K.; Craster, R. V.; Papageorgiou, D. T. Breakup of an electrified viscous thread with charged surfactants. *Phys. Fluids* **2011**, *23*, 022103.

Daga, V. K.; Helgeson, M. E.; Wagner. N. J. Electrospinning of neat and laponite-filled aqueous poly(ethylene oxide) solutions. *J. Polym. Sci. B Polym. Phys*. **2006**, *44*, 1608-1617.

Ekemen, Z.; Ahmad, Z.; Stride, E.; Kaplan, D.; Edirisinghe, M. Electrohydrodynamic bubbling: an alternative route to fabricate porous structures of silk fibroin based materials. *Biomacromolecules*, **2013**, *14*, 1412-1422.

Fernandez de la Mora, J. The effect of charge emission from electrified liquid cones. *J. Fluid Mech*. **1992**, *243*, 561-573.

Fernandez de la Mora, J. The fluid dynamics of Taylor cones. *Annu. Rev. Fluid Mech*. **2007**, *39*, 217-243.

Fernandez de la Mora, J.; Loscertales, I. G. The current transmitted through an electrified conical meniscus. *J. Fluid Mech*. **1994**, *260*, 155-184.

Gamero-Castano, M.; Hruby, B. Electric measurements of charged sprays emitted by cone-jets. *J. Fluid Mech*. **2002**, *459*, 245-276.

Ganan-Calvo, A. M. Revision of capillary cone-jet physics: electrospray and flow focusing. *Phys. Rev. E* **2009**, *79*, 066305.

Ganan-Calvo, A. M. On the theory of electrohydrodynamically driven capillary jets. *J. Fluid Mech.* **1997**, *335*, 165-188.

Graessley, W. W. Polymer chain dimensions and the dependence of viscoelastic properties on the concentration, molecular weight and solvent power. *Polymer* **1980**, *21*, 258-262.

Guo, L.; Bai, J.; Liang, H.; Xu, T.; Li, C.; Meng, Q.; Liu, H.; Huang, Y. A facile approach to preparing palladium nanoparticles-embedded polyvinylpyrrolidone (PVP) heterogeneous hybrid nanofibers mats by electrospinning. *Korean J. Chem. Eng.* **2013**, *30*, 2142-2150.

Gupta, P.; Elkins, C.; Long, T. E.; Wilkes, G. L. Electrospinning of linear homopolymers of poly(methyl methacrylate): exploring relationships between fiber formation, viscosity, molecular weight and concentration in a good solvent. *Polymer* **2005**, *46*, 4799-4810.

Hartman, R. P. A.; Brunner, D. J.; Camelot, D. M. A.; Marijinissen, J. C. M.; Scarlett, B. Electrohydrodynamic atomization in the cone-jet mode physical modeling of the liquid cone and jet. *J. Aerosol Sci.* **1999**, *30*, 823-849.

Hartman, R. P. A.; Brunner, D. J.; Camelot, D. M. A.; Marijinissen, J. C. M.; Scarlett, B. Jet break-up in electrohydrodynamic atomization in the cone-jet mode. *J. Aerosol Sci.* **2000**, *31*, 65-95.

Hashimdeen, S. H.; Miodownik, M.; Edirisinghe, M. J. The design and construction of an electrohydrodynamic Cartesian robot for the preparation of Tissue engineering constructs. *PLoS One* **2014**, *9*, e112166

Hayati, I.; Bailey, A. I.; Tadros, T. F. Mechanism of stable jet formation in electrohydrodynamic atomization. *Nature* **1986**, *319*, 41-43.

Heil, P. E.; Kang, H.; Choi, H.; Kim, K. Effects of controlled surface treatment on titanium dioxide electrode nanostructure for dye-sensitized solar cells. *Appl. Phys. A* **2013**, *112*, 371-380.

Helgeson, M. E.; Grammatikos, K. N.; Deitzel, J. M.; Wagner, N. J. Theory and kinematic measurements of the mechanics of stable electrospun polymer jets. *Polymer* **2008**, *49*, 2924-2936.

Hu, X.; Liu, S.; Zhou, G.; Huang, Y.; Xie, Z.; Jing, X. Electrospinning of polymeric nanofibers for drug delivery applications. J. Control. Release 2014, 10, 12-21.

Hong, S. H.; Moon, J. H.; Lim, J. M.; Kim, S. H.; Yang, S. M. Fabrication of spherical colloidal crystals using electrospray. *Langmuir* **2005**, *21*, 10416-10421.

Higuera, F.J. Breakup of supported drop of a viscous conducting liquid in a uniform electric field. *Phys. Rev. E* **2008**, *78*, 016314.

Jaworek, A & Krupa, A. Classification of the modes of EHD spraying. *J. Aerosol Sci.* **1999**, *30*, 873-893.

Jaworek, A.; Sobczyk, A.T.; Krupa, A.; Lackowski, M.; Czech, T. Electrostatic deposition of nanothin films on metal substrate. Bull. Pol. Ac. 2009, 75, 63-70.

Joffre, G. H.; Cloupeau, M. Characteristic forms of electrified menisci emitting charges. *J. Electrostat*. **1986**, *18*, 147-161.

Kang, D. K.; Lee, M. W.; Kim, H. Y.; James, S. C.; Yoon, S. S. Electrohydrodynamic pulsed-inkjet characteristics of various inks containing aluminum particles. *J. Aerosol. Sci*. **2011**, *42*, 621-630.

Khan, A.; Rahman, K.; Kim, D. S.; Choi, K. H. Direct printing of copper conductive micro-tracks by multi-nozzle electrohydrodynamic inkjet printing process. *J. Mater. Process. Technol*. **2012**, *212*, 700-706.

Khan, A.; Rahman, K.; Hyun M. -T.; Kim, D. -S.; Choi, K. -H. Multi-nozzle electrohydrodynamic inkjet printing of silver colloidal solution for the

fabrication of electrically functional microstructures. *Appl. Phys. A* **2011**, *104*, 1113-1120.

Kim, H. J.; Um, I. C. Relationship between rheology and electro-spinning performance of regenerated silk fibroin prepared using different degumming methods. *Korea-Aust. Rheol. J*. **2014**, *26*, 119-125.

Kim, M. S.; Kim, G. Electrohydrodynamic jet process for pore-structure-controlled 3D fibrous architecture as a tissue regenerative material: fabrication and cellular activities. *Langmuir* **2014**, *30*, 8551-8557.

Korkut, S.; Saville, D. A.; Aksay, I. A. Colloidal cluster arrays by electrohydrodynamic printing. *Langmuir* **2008**, *24*, 13196-12201.

Lannutti, L.; Reneker, D.; Ma, T.; Tomasko, D.; Farson, D.; Electrospinning for tissue engineering scaffolds. Mater. Sci. Eng : C 2007, 27, 504-509.

Lee, A.; Jin, H.; Dang, H. -W.; Choi, K. -H.; Ahn, K. H. Optimization of experimental parameters to determine the jetting regimes in electrohydrodynamic printing. *Langmuir* **2013**, *29*, 13630-13639.

Lee, D. Y.; Hwang, E. S.; Yu, T. U.; Kim, Y. J.; Hwang, J. Structuring of micro line conductor using electro-hydrodynamic printing of a silver nanoparticle suspension. *Appl. Phys. A* **2006**, *82*, 671-674.

Lee, M. W.; Kang, D. K.; Kim, N. Y.; Kim, H. Y.; James, S. C.; Yoon, S. S. A study of ejection modes for pulsed-DC electrohydrodynamic inkjet printing. *J. Aerosol. Sci*. **2012**, *46*, 1-6.

Lee, S.; Kim, J.; Choi, J.; Park, H.; Ha, J.; Kim, Y.; Rogers, J. A.; Paik, U. Patterned oxide semiconductor by electrohydrodynamic jet printing for transparent thin film transistors. *Appl. Phys. Lett*. **2012**, *100*, 102108.

Lee, S. –H.; Nguyen, X. H.; Ko, H.S. Study on droplet formation with surface tension for electrohydrodynamic inkjet nozzle. *J. Mech. Sci. Technol*. **2012**, *26*, 1403-1408.

Li, D.; Xia, Y.; Electrospinning of Nanofibers : Reinventing the Wheel?. *Adv. Mater*. **2004**, *16*, 1151-1170.

Li, J. L. On the meniscus deformation when the pulsed voltage is applied. *J. Electrosta.* **2006**, *64*, 44-52.

Lim, L. K.; Hua, J.; Wang, C. -H.; Smith, K. A. Numerical simulation of cone-jet formation in electrohydrodynamic atomization. *AlChE J.* **2011**, *57*, 57-78.

Mestel, A. J. Electrohydrodynamic stability of a highly viscous jet. *J. Fluid Mech*. **1996**, *312*, 311-326.

Luo, C.J.; Stride, E.; Edirisinghe, M. Mapping the influence of solubility and dielectric constant on electrospinning polycaprolactone solutions. *Macromolecules* **2012**, *45*, 4669-4680.

Mora, J. F. The fluid dynamics of Taylor cones. *Annu. Rev. Fluid Mech.* **2007**, *39*, 217-243.

Mora, J. F.; Loscertales, I. G. The current emitted by highly conducting Taylor cones. *J. Fluid Mech.* **1994**, *260*, 155-184.

Muhammad, N. M.; Sundharam, S.; Dang, H.; Lee, A.; Ryu, B.; Choi, K. CIS layer deposition through electrospray process for solar cell fabrication. *Curr. Appl. Phys.* **2011**, *11*, S68-75.

Nguyen, X. H.; Lee, S. -H.; Ko, H. S. Analysis of electrohydrodynamic jetting behaviors using three-dimensional shadowgraphic tomography. *Appl. Optics* **2013**, *52*, 4494-4504.

Park, J. U.; Hardy, M.; KANG, s. j.; Barton, K.; Adair, K; Mukhopadhyay, D.; Lee, C. Y.; Strano, M. S.; Alleyne, A. G.; Georgiadis, J. G.; Ferreira, P. M.; Rogers, J. A. High-resolution electrohydrodynamic jet printing. *Nat. Mater.* **2007**, *6*, 782-789.

Park, J. U.; Lee, J. H.; Paik, U.; Lu, Y,; Rogers, J. A. Nanoscale patterns of oligonucleotides formed by electrohydrodynamic jet printing with

applications in biosensing and nanomaterials assembly. *Nano Lett*. **2008**, *8*, 4210-4216.

Park, J. -U.; Lee, S. L.; Unarunotai, S.; Sun, Y.; Dunham, S.; Song, T. S.; Ferreira, P. M.; Alleyene, A. G.; Paik, U.; Rogers, J. A. Nanoscale, electrified liquid jets for high-resolution printing of charge. *Nano Lett*. **2010**, *10*, 584-591.

Park, S. E.; Hwang, J. Y.; Kim, K.; Jung, B.; Kim, W.; Hwang, J. Spray deposition of electrohydrodynamically atomized polymer mixture for active layer fabrication in organic photovoltaics. *Sol. Energ. Mat. Sol.* **2011**, *C95*, 352-356.

Qin, X-H.; W, S-Y. Filtration properties of electrospinning nanofibers. J. Appl. Polym. Sci. 2006, 102, 1285-1290.

Regev, O.; Vandebril, S.; Zussman, E.; Clasen, C. The role of interfacial viscoelasticity in the stabilization of an electrospun jet. *Polymers* **2010**, *51*, 2611-2620.

Reneker, D. H.; Yarin, A. L. Electrospinning jets and polymer nanofibers. *Polymer* **2008**, *49*, 2387-2425.

Son, W. K.; Youk, J. H; LEE, T. S.; Park, W. H. The effects of solution properties and polyelectrolyte on electrospinning of ultrafine poly(ethylene oxide) fibers. *Polymer* **2004**, *45*, 2959-2966.

Shenoy, S. L.; Douglas Bates, W.; Frisch, H. L.; Wnek, G. E. Role of chain entanglement on fiber formation during electrospinning of polymer solutions: good solvent, non-specific polymer-polymer interaction limit. *Polymer* **2005**, *46*, 3372-3384.

Stanger, J.; Staiger, M. P.; Tucker, N.; Kirwan, K. An experimental study of the effect of charge density on the Taylor cone in electrospinning. *Solid State Phenom.* **2009**, *151*, 54-59.

Stanger, J.; Tucker, N.; Kirwan, K.; Coles, S.; Staiger, M. P. Effect of charge density on the Taylor cone in electrospinning. *Int. J. Mod. Phys. B* **2009**, *23*, 1956-1961.

Taylor, G. Disintegration of water drops in an electric field. *Proc. R. Soc. London Ser. A* **1964**, *280*, 383-397.

Taylor & Francis Group. The production of nanoparticles: the “Top-Down” approach, with Emphasis on aerosol routes, especially electrohydrodynamic atomization. In Particulate systems in nano- and biotechnologies; Sigmund,

W.; El-Shall, H.; Shah, D. O.; Moudgil, B. M.; *CRC press*: Boca Raton, Florida, **2009**; pp 16-17.

Tapia-Hernandea, J. A.; Torres-Chavez, P. I.; Ramirez-Wong, B. R.; Rascon-Chu, A.; Plascencia-Jatomea, M.; Barreras-Urbina, C. G.; Rangle-Vazquez, N. A.; Rodriguez-Felix, F. J. Agric. Food Chem. 2015, 63, 4699-4707.

Theron, S. A.; Zussman, E.; Yarin, A. L. Experimental investigation of the governing parameters in the electrospinning of polymer solutions. *Polymer* **2004**, *45*, 2017-2030.

Tirtaatmadja, V.; McKinley, G. H.; Cooper-Whith, J. J. Drop formation and breakup of low viscosity elastic fluids: effects of molecular weight and concentration. *Phys. Fluids* **2006**, *18*, 043101.

Wang, K.; Paine, M.D.; Stark, J. P. W. Fully voltage-controlled electrohydrodynamic jet printing of conductive silver tracks with a sub-100 μm linewidth. *J. Appl. Phys*. **2009**, *106*, 024907.

Wei, W.; Gu, Z.; Wang, S.; Zhang, Y.; Lei, K.; Kase, K. Numerical simulation of the cone-jet formation and current generation in electrostatic spray-modeling as regards space charged droplet effect. *J. Micromech. Microeng*. **2013**, *23*, 015004.

Xu, L.; Wang, X.; Lei, T.; Sun, D.; Lin L. Electrohydrodynamic deposition of polymeric droplets under low-frequency pulsation. *Langmuir* **2011**, *27*, 6541-6548

Yang, T.; Yao, Y.; Lin, Y.; Wang, B.; Xiang, R.; Wu, Y.; Wu, D. Electrospinning of polyacrylonitrile fibers from ionic liquid solution. *Appl. Phys. A* **2010**, *98*, 517-523.

Yordem, O. S.; Papila, M.; Menceloglu, Y. Z. Effects of electrospinning parameters on polyacrylonitrile nanofiber diameter: An investigation by response surface methodology. *Mater. Des.* **2008**, 29, 34-44.

Yu, J.H.; Kim, S. Y.; Hwang, J. Effect of viscosity of silver nanoparticle suspension on conductive line patterned by electrohydrodynamic jet printing. *Appl. Phys. A* **2007**, *89*, 157-159.

Yurteri, C. U.; Hartman, R. P. A.; Marijnissen J. C. M. Producing pharmaceutical particles via electrospraying with an emphasis on nano and nano Structured Particles - A Review. *KONA.* **2010**, *28*, 91-115.

Zeleny, J. The electrical discharge from liquid points, and a hydrostatic method of measuring the electric intensity at their surfaces. *J. Phys. Rev.* **1914**, *3*, 69-91.

Zeleny, J. Instability of electrified liquid surfaces. *J. Phys. Rev*. **1917**, *10*, 1-6.

Zong, X.; Kim, K.; Fang, D.; Ran, S.; Hsiao, B. S.; Chu, B. Structure and process relationship of electrospun bioabsorbable nanofiber membranes. *Polymers* **2002**, *43*, 4403-4412

국문 초록

전자부품의 소형화 추세에 대응하여 나노 패턴을 생성할 수 있는 전기수력학 프린팅이 촉망 받는 인쇄전자 기술로 대두되고 있다. 전기수력학 프린팅으로 고해상도 패턴을 생성하기 위해서는 테일러 콘 젯을 형성하는 것이 중요하다. 테일러 콘 젯은 공정 변수, 장비 변수 그리고 잉크의 물성 (탄성, 점성, 전도도, 표면장력 그리고 유전율)에 의해서 영향을 받는다. 특히, 잉크는 입자, 고분자, 용매를 포함하는 복합유체로서 점탄성이 중요한 요소임에도 불구하고, 기존 연구에서는 단순한 뉴토니안 유체를 잉크로 가정해왔다. 균일하고 높은 해상도의 패턴을 인쇄하기 위해서는 테일러 콘 젯 형성에 적합한 점탄성 잉크의 물성과 공정 조건을 예측하고 제어하는 것이 중요하다. 그러므로, 본 연구에서는 전기수력학 프린팅에 적합한 점탄성 유체의 유변학적 그리고 전기적 물성이 테일러 콘 젯 형성에 미치는 영향을 조사함으로써, 고해상도 패턴 인쇄에 적합한 잉크의 물성을 설계하고 공정 조건을 최적화 하였다.

우선, 테일러 콘 젯에 영향을 주는 변수를 체계화하기 위해 전기수력학 프린팅 공정에 영향을 미치는 모든 변수를 고려하여

일곱 개의 무차원 수를 구성하였다. 이 중, 무차원 유량(α)과 무차원 전압(β)은 무차원 공정 변수로 사용되었고, 잉크의 물성을 대표하는 두 무차원 수인 탄성 지표(ξ)와 점성 지표(χ)는 잉크의 탄성과 점성이 테일러 콘 젯 형성에 영향을 미치는 여부를 판단할 수 있는 중요한 변수로 제시되었다. 탄성과 점성을 독립적으로 제어한 두 개의 모델 시스템을 구성함으로써 탄성 지표(ξ)와 점성 지표(χ)를 조절하였다. 탄성의 증가는 테일러 콘 젯을 형성하는 전압 범위를 증가시킨 반면, 유량 범위에는 영향을 미치지 않았다. 특히, 탄성의 증가는 테일러 콘 젯을 형성하는 초기 전압과 밀접한 연관이 있음을 관찰하였다. 이를 통해 탄성의 증가가 테일러 콘 젯 표면에 내부 법선 방향의 응력을 증가시켰음을 알 수 있었다. 이러한 탄성의 효과는 ξ 가 1 보다 클 때 우세하게 나타나며, ξ 가 1 보다 작은 경우에는 그 효과가 거의 나타나지 않았다. 점도의 증가는 테일러 콘 젯이 형성되는 공정 영역을 증가시켰는데, χ 가 1 보다 작은 영역에서는 유량의 범위가 증가하였고 χ 가 1 보다 큰 영역에서는 전압의 범위가 증가하였다. 결과적으로 점탄성의 증가는 콘 젯 형상에 안정성을 부여해, 테일러 콘 젯이 형성되는 공정 범위를 증가시킴을 알 수 있었다.

다음으로, 잉크의 유변 물성과 전기적 물성을 모두 제어한 모델시스템을 통해서 유변 물성과 전기적 물성의 상호작용이

테일러 콘 젯의 공정 조건에 미치는 영향을 조사하였다. 전도도가 높은 잉크일수록 표면 넓이가 큰 콘 형상을 생성하는 것이 관찰되었다. 콘 젯을 형성하기 위해 넓은 표면에 더 많은 양의 전하 축적이 요구되어, 테일러 콘 젯이 발생하는 초기 전압이 높아졌다. 테일러 콘 젯 형성 이후에는 콘 형상에 안정성을 부여하면서 더 높은 전압까지 콘 형상을 유지시켜 최대 전압의 값을 높였다. 전기적 물성이 동일하게 증가할 경우, 탄성과 점성이 높은 잉크일수록 테일러 콘 젯을 형성할 수 있는 전압 영역이 줄어듦이 관찰되었다. 이는 탄성과 점성의 증가가 콘 젯 내부 유동 하에서 전하의 이동을 방해함으로써 나타난 현상으로 해석된다. 결과적으로, 잉크의 유변물성과 전기적 물성의 변화가 테일러 콘 젯에 작용하는 메커니즘은 다르나, 테일러 콘 젯이 발생하는 공정 영역 변화에 있어서는 초기 전압과 최대 전압을 증가시키는 동일한 양상을 보임을 알 수 있었다.

본 연구는 전기수력학 프린팅 공정에서 발생하는 테일러 콘 젯 형성에 적합한 점탄성 잉크의 물성을 디자인하고 공정을 최적화하는 가이드라인을 제시하였다. 공정에 영향을 미치는 모든 변수를 차원 해석을 통해 체계화하였다. 잉크의 유변 그리고 전기적 물성을 제어한 모델시스템을 통해 각 물성이 테일러 콘 젯에 미치는 영향을 조사하였다. 점탄성 잉크의 물성 변화에 따라

발생하는 젯팅 모드를 무차원 공정 변수인 무차원 유량(α)과 무차원 전압(β)에 대한 공정 맵으로 도시함으로써 잉크 물성과 공정 조건에 따른 테일러 콘 젯 형성 영역을 나타내었다. 이 연구 결과는 잉크 물성이 공정 중 나타내는 거동을 이해하고 실제 고해상도 패턴을 인쇄하기 위한 공정 범위를 체계적으로 예측할 수 있는 플랫폼이 될 수 있을 것 이라고 생각한다.

주요어: 전기수력학 프린팅, 테일러 콘 젯, 점탄성 잉크, 유변 물성, 전도도, 무차원 변수, 공정 맵, 고해상도 패턴

학 번: 2008 – 22982